Influence of permafrost, rock and ice glaciers on chemistry of high-elevation ponds (NW Italian Alps)

Influence of permafrost, rock and ice glaciers on chemistry of high-elevation ponds (NW Italian Alps)

N. Colombo[a], F. Salerno[b,*], M. Martina[a], M. Malandrino[c], M. Giardino[d], E. Serra[e], D. Godone[f], D. Said-Pullicino[a], S. Fratianni[d], L. Paro[g], G. Tartari[b], M. Freppaz[a]

[a]University of Turin, Department of Agricultural, Forest and Food Sciences, Grugliasco, Italy.
[b]CNR-IRSA (National Research Council - Water Research Institute), Brugherio, Italy.
[c]University of Turin, Department of Chemistry, Turin, Italy.
[d]University of Turin, Department of Earth Sciences, Turin, Italy.
[e]University of Bern, Institute of Geological Sciences, Bern, Switzerland.
[f]CNR-IRPI (National Research Council - Research Institute for Geo-Hydrological Protection), Turin, Italy.
[g]Arpa Piemonte, Department of "Natural and Environmental Risks", Turin, Italy.
Corresponding author: Franco Salerno (salerno@irsa.cnr.it)

Highlights

- Chemical weathering varies under different cryospheric conditions in mountain areas.
- Higher seasonal increases in major ions in ponds with cryospheric features.
- Sulphide oxidation dominates in glacier and permafrost lying on acid rocks.
- Carbonation dominates in the rock glacier lying on ultramafic rocks.

Graphical abstract

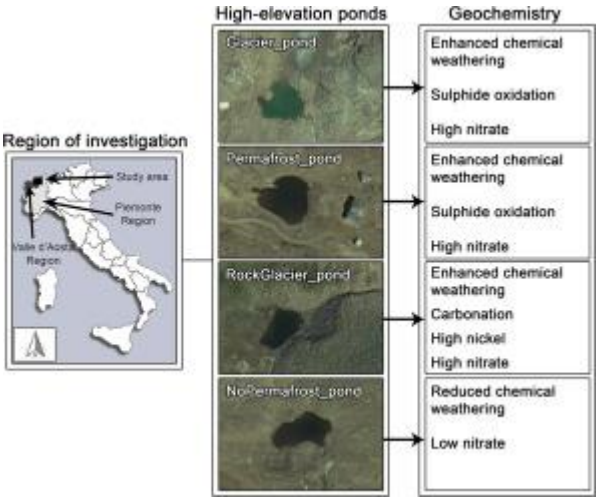

Abstract

Permafrost degradation, rock-glacier thawing, and glacier retreat are influencing surface water quality at high elevations. However, there is a lack of knowledge on the dominant geochemical reactions occurring in different cryospheric conditions and how these reactions change during the ice-free season. In the Col d'Olen area (LTER site, NW Italian Alps), four ponds with similar sizes, located in basins with different cryospheric features (glacier, permafrost, rock glacier, none of these), are present in a geographically limited area. All ponds were sampled weekly in 2015 and partially in 2014. Major ions, selected trace elements, and biotic parameters (dissolved organic carbon-DOC, fluorescence index-FI, and nitrate) are examined to evidence the effect of different cryospheric features on water characteristics. Where cryospheric conditions occur chemical weathering is more intensive, with strong seasonal increase of major ions. Sulphide oxidation dominates in glacier and permafrost lying on acid rocks, probably driven by enhanced weathering of freshly exposed rocks in subglacial environment and recently deglaciated areas, and active layer thickness increase. Differently, carbonation dominates for the rock glacier lying on ultramafic rocks. There, high Ni concentrations originate from dissolution of Mg-bearing rocks in the landform. In all settings, pH neutralisation occurs because of the presence of secondary carbonate lithology and ultramafic rocks. Nitrate highest concentrations and changes occur in cryospheric settings while DOC and FI do not show strong differences and seasonal variations. The establishment of more frequent monitoring for water quality in high-elevated surface waters is necessary to provide greater statistical power to detect changes on longer time scales.

Keywords

Water chemistry; Alps; Weathering; Cryospheric features; LTER; Soil

1. Introduction

During the last two decades the majority of glaciers have been retreating and losing mass in all high-mountain regions (Zemp et al., 2015; Colombo et al., 2016a), and permafrost has undergone warming, degradation, and ice loss (Harris et al., 2003; Gruber et al., 2017). The observed changes in the cryosphere are influencing the surface water chemistry (Colombo et al., 2018a). Increases in solutes have been attributed to permafrost degradation (Mast et al., 2011; Todd et al., 2012), rock-glacier thawing (Ilyashuk et al., 2014, Ilyashuk et al., 2018), and glacier melting (Fortner et al., 2011; Salerno et al., 2016). Permafrost degradation has been reported to impact surface water quality in different areas of the world such as in the Arctic (e.g., Roberts et al., 2017; Szumińska et al., 2018), Antarctic (e.g., Levy et al., 2011; Gooseff et al., 2016), and several mountain ranges (e.g., Szopińska et al., 2016; Toohey et al., 2016). Moreover, water originating from rock glaciers has been shown to contain high heavy metal concentrations, mainly nickel, exceeding the guideline values for drinking water quality (Thies et al., 2013; Ilyashuk et al., 2014). Also nitrogen (N) forms and dissolved organic carbon (DOC) are predicted to increase with glacier shrinkage (Hood et al., 2015; Milner et al., 2017) and permafrost degradation (Baron et al., 2009; Abbott et al., 2014).

It is now evident that cryospheric features are capable of strongly influencing the chemical quality of surface water bodies. However, comprehensive investigations on the dynamics of high-elevation surface waters characterised by different cryospheric conditions are uncommon and geographically scattered (Williams et al., 2006; Fegel et al., 2016). Moreover, there is a paucity of studies on how different cryospheric features influence the dynamics of biotic parameters such as dissolved inorganic N and DOC in high-elevation surface waters (Williams et al., 2007; Fegel et al., 2016).

Usually, water bodies located in high-mountain environments are characterised by small dimensions, and can be defined as "ponds" according to Hamerlík et al. (2014) (a threshold of 2×104 m2 exists between ponds and lakes). Ponds represent key investigation sites of surface water quality at high elevations due to minimal direct human influence and because of their rapid response to climate-related changes (Adrian et al., 2009; Salerno et al., 2014). Moreover, at a temporal resolution of weekly observations, ponds have the advantage of integrating signals, which in streams might otherwise vary too quickly to be adequately appreciated (Salerno et al., 2016; Colombo et al., 2018b, Colombo et al., 2018c).

The Col d'Olen area (LTER site Istituto Mosso - NW Italian Alps) can be considered as an excellent site for investigating the relationships between cryospheric and surface water dynamics. The aim of this work is to provide new insights into the geochemical reactions occurring in different cryospheric conditions and how these reactions change during the ice-free season (pond surface without ice cover). We evaluated the dynamics of pond water characteristics during the ice-free season in four ponds with similar sizes, present in a geographically limited area (similar morpho-climatic conditions) at an elevation >2700 m a.s.l., and located in basins characterised by different cryospheric features (ice glacier, permafrost, rock glacier, none of these). All ponds were sampled weekly in 2015 and partially in 2014 (only the glacier and rock-glacier ponds were sampled), during the ice-free season. Major ions, selected trace elements, and biotic parameters are discussed here in order to evidence the effect of different cryospheric features on pond water characteristics.

2. Materials and methods

2.1. Study area

The four investigated ponds are located in the NW Italian Alps, along Valle d'Aosta and Piemonte regional border, close to the Monte Rosa massif (Fig. 1). The research site is a node of the LTER network in Italy (http://www.lteritalia.it). Maximum linear distance among ponds is approximately 2.5 km, while their elevation ranges between 2722 and 3083 m a.s.l.

A glacier (Indren Glacier) is located in the Indren Pond basin, in direct contact with the pond. Permafrost probably occurs in the Bowditch Pond basin, which is located in the uppermost area of the Cimalegna plateau. A talus-tongue-shaped rock glacier (more information about the rock glacier can be found in Colombo et al., 2018b, Colombo et al., 2018c) flows into the Olen Pond. The above mentioned cryospheric features are absent in the Cimalegna Pond basin, located in the middle area of the Cimalegna plateau (Fig. 1). The selected ponds will hereafter be named Glacier_pond, Permafrost_pond, RockGlacier_pond, and NoPermafrost_pond, respectively, as a function of the prevalent cryospheric features in their basin (Fig. 1). Morphometric characteristics of these ponds and relative basins are reported in Table 1. All ponds do not have persistent surface inflows, while they all have surface outflows except for the RockGlacier_pond (Colombo et al., 2018b, Colombo et al., 2018c).

The geological maps elaborated by the Valle d'Aosta Region (scale 1:10,000, source: http://geologiavda.partout.it/) and by Leonoris et al. (2009), supported by several field surveys in 2014 and 2015, show that the bedrock of the pond basins is mainly characterised by metamorphic rocks (Fig. 2a1–a4). Glacier_pond, Permafrost_pond, and NoPermafrost_pond basins display the predominant presence of rocks with acid composition, with secondary presence of basic and terrigenous carbonatic rocks. Differently, the RockGlacier_pond basin is mainly characterised by basic and ultrabasic rocks, with secondary presence of terrigenous carbonatic and acid rocks (further details in Supplementary Material (S), Study area S1); the fine-grained deposit constituting the interior of the rock glacier, where outcropping, is composed by serpentinites while the surface of the landform is covered by clasts (gravel to boulders) of calcschists and serpentinites (Colombo et al., 2018c).

The land cover characteristics of the basins were mapped by photointerpretation of digital orthoimages (years 2006 and 2012), supported by several field surveys (years 2014 and 2015). From the mapping activity, three main categories were identified within the basin area: (i) bedrock, (ii) coarse sediment, and (iii) soil. The land cover of the Glacier_pond basin is dominated by the glacier (Fig. 2b1). Coarse sediment constitutes the main land cover type in the Permafrost_pond and RockGlacier_pond basins (Fig. 2b2, b3). Differently, soil (often vegetated) is the main land cover type in the NoPermafrost_pond basin (Fig. 2b4). In all basins, bedrock outcrop is the second most widespread land cover type.

2.2. Meteorological measurements and cryospheric features

For the 2008–2015 period, an automatic weather station located close to the Permafrost_pond (AWS, Col d'Olen station, 2901 m a.s.l., operated by Comando Truppe Alpine - Ufficio Meteomont, Fig. 1) recorded a mean annual air temperature of −2.6 °C, a mean cumulative snowfall equal to 850 cm, and a mean liquid precipitation during the ice-free season of 400 mm. The snowpack generally developed by late October to early November, and melt out occurred mainly from July. Daily rain data for the investigated period were obtained from the Gressoney-La-Trinité - Lago Gabiet AWS (2379 m a.s.l., operated by Valle d'Aosta Region), located at ca. 3 km distance from the Col d'Olen AWS. Estimation of presence/absence of snowpack was based on two different approaches: (i) local meteorological measurements obtained from the Col d'Olen AWS (daily measurements), and (ii) spatially distributed approach based on Landsat 8 (weekly to bi-weekly observations) (Materials and Methods S2.1). Furthermore, among large blocks of the rock glacier, a fine-scale spatially distributed analysis of long-lasting snow patches was performed (further details in Colombo et al., 2018c).

To investigate the cryospheric conditions in the basins, different methods were used. (i) The potential permafrost distribution was investigated using the Alpine Permafrost Index Map (APIM, Boeckli et al., 2012a) (Fig. 2c1–4) (Materials and Methods S2.1). (ii) Ground surface temperature (GST, e.g., Ishikawa, 2003) data were used to integrate the information obtained by the APIM. Temperature sensors were installed in the period 2015–2016 in the most representative debris deposits of each basin (Fig. 2b1–b4), while a longer data series is available for the NoPermafrost_pond basin (2008–2015) (Materials and methods Section 2.1). To assess the ground thermal regime, and the possible occurrence of permafrost, relevant parameters were extracted from the GST data, such as mean annual ground surface temperature (MAGST), ground freezing index (GFI), and winter equilibrium temperature (WEqT) (e.g., Seppi et al., 2015). (iii) To further investigate the ground surface thermal conditions in the Permafrost_pond basin and on the slopes above the NoPermafrost_pond basin, bottom temperature of the snow cover (BTS, e.g., Hoelzle, 1992) measurements were performed in 2013 and 2014 (Materials and Methods S2.1). (iv) Ground temperature (GT) data from a 30-m deep borehole managed by Arpa Piemonte in the southern slope of the Permafrost_pond basin at 3020 m a.s.l. (Paro and Guglielmin, 2013) (Fig. 2b2) were used to analyse the ground thermal conditions.

2.3. Pond water and precipitation sampling, and chemical analysis

During the ice-free season 2015 (July–October) all ponds were sampled weekly for a total of about 14 samples for each pond. Due to technical problems, trace elements were not analysed for the sampling performed on 7 August 2015. In 2014 (August–October), only the Glacier_pond and RockGlacier_pond were sampled, for a total of about 8 samples for each pond. All ponds were sampled from a point on the shore with no vegetation, using a telescopic sampling beam (Fig. 1). Water samples taken from shore were assumed not to be significantly different from mid-pond samples because the investigated ponds are small and shallow (Mast et al., 2011). Furthermore, a 300 cm-deep snow profile was sampled before the melting season near the Col d'Olen AWS in April 2015 (Fig. 1), and 6 snow samples were collected at 50-cm intervals for chemical analyses (Materials and Methods Section 2.2). Finally, a rain collector was installed in July 2015 closed to the RockGlacier_pond (Fig. 1) and sampled when precipitation occurred (5 observations).

pH was measured potentiometrically (WTW-InoLab 7110 pH-meter equipped with Hamilton GelGlass electrode). Electrical conductivity (EC) at 20 °C was measured using a Crison - Micro CM 2201. The concentration of major anions (Cl^-, NO_2^-, NO_3^-, PO_4^{3-}, SO_4^{2-}) was determined by ion

chromatography (Dionex DX-500, California), while major cations (Ca2+, Mg2+, K+, Na+) were determined by flame atomic absorption spectroscopy (Perkin Elmer AAnalyst 400, Waltham, Massachusetts). Si and potentially toxic trace elements (Ni, Mn, Co, coming from the weathering of basic and ultrabasic rocks, e.g., Brooks, 1987), of relevance in the investigated area, were determined by inductively coupled plasma-sector field mass spectrometry (Thermo Finnigan Element 2, Bremen, Germany). Ammonium (NH4+) concentrations were determined spectrophotometrically (U-2000, Hitachi, Tokyo, Japan) by a modified Berthelot method involving reaction with salicylate in the presence of alkaline sodium dichloroisocyanurate (Crooke and Simpson, 1971). The quality of chemical analyses was determined by including method blanks, and repeated measurements of standard reference samples and certified samples (NIST 1640 "Trace elements in natural water"). Analytical precision for major anions was <10%, and for major cations and for trace elements was <5%. Total carbon (TC) and dissolved inorganic carbon (DIC, here expressed as HCO3−) (further analytical details can be found in Polesello et al., 2006) were analysed with a VarioTOC (Elementar, Hanau, Germany). Dissolved organic carbon (DOC) was quantified from the difference between TC and DIC. Fluorescence measurements were conducted on the DOC in the water samples using a HORIBA Scientific FluoroMax 3 (Materials and Methods S2.2). Analytical precision for DOC, HCO3−, and fluorescence index-FI was <2%. To investigate the differences in the dominant weathering processes, S-ratio [SO42−/(HCO3− + SO42−)] and Mg-ratio [Mg2+/(Ca2+ + Mg2+)] (where units of concentrations are expressed in equivalents per liter and the ratio as percentage) were calculate.

Charge balance errors (CBE), expressed as percentages, were calculated as follows:

$$\mathrm{CBE} = \frac{\left(\sum^{+} - \sum^{-}\right)}{\left(\sum^{+} + \sum^{-}\right)} \times 100\%$$

where $\sum^{+}$ is the sum of the cation (eq. L^{-1}) and $\sum^{-}$ is the sum of the anion (eq. L^{-1}). The mean CBE values were: Glacier_pond, −11%; Permafrost_pond, −7%; RockGlacier_pond, +5%; NoPermafrost_pond, −1%; snow, +13%; and rain, +10%.

DOC, FI, and NO3− were considered as “biotic parameters”. Indeed, previous studies in cryospheric settings considered these parameters as specific marker of microbial activity (Williams et al., 2007; Hood et al., 2009; Bhatia et al., 2013), with DOC and NO3− released from cryospheric features also able to influence the downstream ecosystems (Slemmons et al., 2013; Fegel et al., 2016; Milner et al., 2017).

2.4. Statistical analysis

Differences in the temporal variation of chemical constituents during the sampling period were evaluated by pooling together the data collected in three selected periods of the ice-free season 2015: early (9, 15, 20 July), middle (13, 24, 31 August), and late (21, 28 September, and 5, 12 October) ice-free season. The normality of the data was tested using the Shapiro-Wilk test. The data were also tested for homogeneity of variance with the Levene's test. To evaluate the significance of differences in solute concentration for the different sampling periods, one-way analysis of variance (ANOVA) was applied if data were normally distributed. In case of non-normally distributed data, the Kruskal-Wallis test was applied. All tests were implemented in the R software (R Core Team, 2019) with the significance level at $p < 0.05$.

3. Results

3.1. Meteorological conditions and cryospheric characteristics of ponds basins

The Col d'Olen AWS showed the absence of the snowpack at the beginning of monitoring (July 2015) (Fig. 3a), while a rather thick early-fall snowpack started developing at the end of sampling (October 2015). Landsat data confirmed the absence of snow in the basins until the beginning of October 2015. Among the blocks of the rock glacier, snowpack depletion occurred before the start of the sampling season (Colombo et al., 2018c). In July–August 2015, the mean air temperature was +6.4 °C (Fig. 3b), while it became negative or around 0 °C in September and during the first half of October (mean: −0.2 °C). During the ice-free season, six main precipitation events occurred, mainly concentrated in August (i.e, in the middle ice-free season). A main snow event occurred at the beginning of October.

According to the APIM (Permafrost Index – PI, Table 1) and its interpretation key (Boeckli et al., 2012a), permafrost is presumably present in the steep rock walls and coarse debris deposits in the basins of the Glacier_pond, Permafrost_pond, and RockGlacier_pond (Fig. 2c1–3). Permafrost is likely

to be absent in the soil and flat-bedrock outcrop areas of the NoPermafrost_pond and RockGlacier_pond basins (Fig. 2c3–4), as well as below the temperate (Maggioni et al., 2009), wet-based Indren Glacier (cf., Haeberli and Gruber, 2008).

The thermal regime of the ground surface in the four basins is shown in Fig. 4 (sensors locations in Fig. 2b1–b4), along with the evolution of the air temperature and the snowpack. MAGST and GFI in the Glacier_pond indicate very cold thermal conditions of the ground surface (Fig. 4, Table S2). In the Permafrost_pond, GST data confirm the possible presence of permafrost at the monitoring site (e.g., Seppi et al., 2015) with negative WEqT and GFI (Fig. 4, Table S2). Decidedly negative MAGST, GFI and WEqT confirm the presence of permafrost in the rock glacier, showing the well-known "negative thermal anomaly" characterising this coarse deposit (e.g., Harris and Pedersen, 1998), especially evident if compared to the warmer conditions characterising the soil-covered areas in the landform surroundings (Fig. 4, Table S2). Finally, although the NoPermafrost_pond is located close to the Permafrost_pond (i.e., elevation difference of 100 m only), the cryospheric conditions of its basin appear remarkably different. Indeed, GST data exclude the occurrence of permafrost in the NoPermafrost_pond basin, with WEqTs close to 0 °C, decidedly positive MASGTs, and slightly negative GFI values (Fig. 4, Fig. S1, Table S2).

The BTS measurements performed in the Permafrost_pond basin and on the slopes above the NoPermafrost_pond basin (Fig. 4) highlight the great thermal difference between these two areas. The BTS measurements showed very cold ground surface conditions in the higher, southern slopes of the Permafrost_pond basin, indicating the likely presence of permafrost (cf., Julián and Chueca, 2007). This is confirmed by the 30-m deep borehole data, indicating the presence of warm permafrost (close to 0 °C) in this site, with a maximum active layer thickness (ALT) of 3 m (late October 2014) and 4 m (early October 2015) (Fig. 4). BTS values gradually became warmer towards the northern zone of the Permafrost_pond basin and towards the eastern slope, in the transitional zone of the Permafrost_pond and NoPermafrost_pond basins, indicating the progressive disappearance of permafrost. The absence of permafrost in the NoPermafrost_pond basin could be explained by gentle slopes which favour snow accumulation and related thermal buffer effect, and presence of vegetated soil (Goodrich, 1982; Zhang et al., 1997). Moreover, permafrost absence is consistent with the observations showing that alpine permafrost is more common in areas of large-grain sizes than of fine-grained materials (e.g., Boeckli et al., 2012b).

3.2. Chemical characteristics of ponds and precipitation

Table 2 presents the statistical summary of the chemical characteristics of ponds, snow and rain during the ice-free season 2015. The observed chemical trends are shown in Fig. 5 for 2015, and in Fig. S2 for 2014. Possible significant differences among early, middle, and late ice-free season are presented in Table S1.

The main results related to the pond water quality are presented below.

1. The Permafrost_pond showed the highest mean EC (84 μS cm−1), while the lowest mean value was measured at the NoPermafrost_pond (36 μS cm−1) (Table 2). Greatly lower mean values were measured in snow and rain (4 and 7 μS cm−1, respectively). All ponds, except the NoPermafrost_pond, showed strong EC increases during the ice-free season (Fig. 5a, Table S1). The highest values were observed during the late ice-free season at the Glacier_pond and Permafrost_pond, and during the middle ice-free season at the RockGlacier_pond. These ponds evidenced mean EC values up to 3 times higher than ones recorded during the early ice-free season.

2. The mean pH of four ponds ranged from neutral (7) to subalkaline (7.5), while snow and rain presented more acidic values (5.6 and 6.0, respectively) (Table 2). All ponds showed pH increases during the ice-free season (Fig. 5b), with stronger variations at the Glacier_pond, Permafrost_pond, and RockGlacier_pond (Table S1).
3. For all ponds, SO_4^{2-} and HCO_3^- were the dominant anions, while Ca^{2+} and Mg^{2+} were the prevailing cations (Fig. 6). The highest EC at the Permafrost_pond corresponded to the highest concentrations of SO_4^{2-} (455 μeq L^{-1}) and Ca^{2+} (470 μeq L^{-1}), while at the NoPermafrost_pond the concentrations of SO_4^{2-} (104 μeq L^{-1}) and Ca^{2+} (209 μeq L^{-1}) were respectively ca. 4-fold and 2-fold lower than the ones found at the Permafrost_pond (Table 2). According to the EC, concentrations of dominant anions and cations increased during the ice-free season. Glacier_pond and Permafrost_pond showed the highest values during the late ice-free season, and the RockGlacier_pond during the middle ice-free season, while slight or no increases were observed at the NoPermafrost_pond (Fig. 5c, d, e, Table S1).
4. During the early ice-free season, the RockGlacier_pond showed an S-ratio decidedly lower (12%) than the other ponds (43% - Glacier_pond, 51% - Permafrost_pond, 39% - NoPermafrost_pond) (Fig. 6). In all ponds, excluding the NoPermafrost_pond, the S-ratio markedly increased during the ice-free season (71% - Glacier_pond, 69% - Permafrost_pond, 24% - RockGlacier_pond).
5. During the early ice-free season, the RockGlacier_pond showed an Mg-ratio decidedly higher (46%) than the other ponds (23% - Glacier_pond, 15% - Permafrost_pond, 17% - NoPermafrost_pond) (Fig. 6). The Mg-ratio increased in all ponds during the ice-free season, with the highest increase measured at the RockGlacier_pond in the middle ice-free season.
6. Among the potentially toxic trace elements, Ni was the dominant one for all ponds with a mean concentration at the RockGlacier_pond (340 nmol L^{-1}) approximately one order of magnitude higher than concentrations in the other ponds (Table 2). Here, the highest concentrations were observed during the middle ice-free season (Fig. 5g, Table S1).
7. Among the biotic parameters, the NoPermafrost_pond showed the lowest mean NO_3^- concentration (4 μeq L^{-1}), which was less than half observed in the other ponds (Table 2). At all sites, NO_3^- concentrations increased significantly during the middle ice-free season (Fig. 5h, Table S1). After this period, NO_3^- concentrations decreased, especially at the RockGlacier_pond and NoPermafrost_pond, with concentrations in the two ponds approaching similar values in the late ice-free season.

8. Differently, mean concentrations as well as temporal variations of DOC and FI did not show any clear difference among ponds and seasonal trends (Table 2, Fig. 5i, l, Table S1). However, the Glacier_pond and RockGlacier_pond displayed the highest seasonal variability for FI.

4. Discussion

4.1. Factors potentially influencing the water quality of the ponds

To understand the difference in the water chemical quality of the ponds, the most important factors potentially influencing the chemical characteristics of high-mountain waters are discussed here.

4.1.1. Atmospheric deposition

Given the low weathering-derived solute content in the atmospheric deposition with respect to the pond water (Table 2), the chemistry of the ponds can be mainly attributed to chemical weathering of rocks and soils. Moreover, considering the geographically limited area of investigation, the effect of atmospheric deposition should be similar for all ponds, thus the observed differences among the ponds should be attributed to other factors.

4.1.2. Climate

The similarly sized ponds are located in a geographically limited area with reduced elevation differences. Therefore, climatic conditions such as liquid precipitation, air temperature and consequent evaporative processes can be assumed to be similar among the selected basins. Generally, snow is considered as an important factor driving the seasonality of high-elevated surface waters, reducing solute concentrations during the early ice-free season, after the ionic pulse occurring at the beginning of the snow melting season (e.g., Williams and Melack, 1991). In our case, the snow conditions were very similar in all basins (Fig. 3). Hence, snow duration cannot be considered as the main reason for the observed differences in solute trends among the ponds.

4.1.3. Soil distribution

The presence of soil is generally associated with higher release of weathering-derived solutes in surface waters due to a significantly higher mineral surface area exposed to weathering than in coarse deposits

and bedrock, and a higher residence time of water in contact with weatherable minerals in the soil (e.g., Drever and Zobrist, 1992; Marchetto et al., 1995). The NoPermafrost_pond belongs to the basin with the highest surface covered by soil (Fig. 2b4). Considering that its solute concentrations (Table 2) and seasonal variations (Fig. 5, Table S1) were the lowest among the ponds, the abundance of soil in the basin cannot be considered as a key factor in explaining the observed differences.

4.1.4. Lithology

Main differences in the lithology of the basins exist between the RockGlacier_pond basin and the other basins. Indeed, metamorphic rocks with basic/ultrabasic composition and schistous texture (serpentinites, serpentineschists) are abundant only in the RockGlacier_pond basin (Fig. 2) and constitute the fine-grained material in the inner part of the landform. This difference is reflected in the water quality of the RockGlacier_pond. Indeed, the RockGlacier_pond shows an Mg-ratio of ca. 50% due to high Mg^{2+} release from ultrabasic rocks, while for the other basins the ratio is ca. 20% (Fig. 6). For the same reason, high Ni concentrations (average: 340 nmol L^{-1}, Table 2) occurred in the RockGlacier_pond (c.f., Kandji et al., 2017).

4.1.5. Hydrology

Regarding the Permafrost_pond, air temperature during the summer is generally considered to be the main driver of active layer evolution in mountain permafrost (e.g., Harris et al., 2009), with the maximum ALT generally reached between September and November (e.g., PERMOS, 2016). Maximum sub-surface discharge from permafrost has been estimated to occur when ALT is at its maximum (Ge et al., 2011). In the Permafrost_pond basin borehole, maximum ALT in 2015 was reached at the beginning of October. For this reason, it is possible to assume that, at the end of the ice-free season 2015, the hydrochemical fluxes from the Permafrost_pond basin into the pond where higher, thus explaining the increasing solute concentrations in September and October (Fig. 5, Table S1). Progressively increasing seasonal solute concentrations at the Permafrost_pond are in agreement with previous studies performed in other mountain ranges that found increasing weathering signals in surface water attributable to permafrost thawing as the summer progressed (e.g., Beylich et al., 2003; Keller et al., 2010). Interestingly, the last two water samples (5 and 12 October) showed rather lower solute concentrations (well represented by EC values) (Fig. 5). In this case, it is possible that increasing

solute concentrations due to maximum ALT were counterbalanced by the partial melting of the solute-diluted early fall snowpack (Fig. 3).

With regard to the Glacier_pond, a direct relationship between glacier discharge and air temperature is widely reported in literature as the basic climatic influence on glacier melting processes (e.g., Hock, 2003). Furthermore, solute concentrations are often inversely related with glacier runoff, so that a rough rule of thumb is that low-discharge waters are concentrated whereas high-discharge waters are diluted (Tranter, 2006; Yde, 2011). The generally decreasing air temperature trend observed from the early to the late ice-free season might have been reasonably linked to a decrease in glacier melting and an increase in solute concentrations (Fig. 5, Table S1).

A greater hydrological knowledge is currently available for the RockGlacier_pond. Colombo et al. (2018b) estimated the rock-glacier inflow contribution to the pond through heat tracing methods. A general decreasing rock-glacier discharge trend was observed between the early and late ice-free season 2015. The contribution from the rock glacier reached minimum values when the mean air temperature was negative or close to 0 °C (Fig. 3). This observation agrees with the results obtained by previous studies on rock-glacier hydrology reporting a direct relationship between air temperature and rock-glacier discharge (Krainer et al., 2007; Geiger et al., 2014). Therefore, the decreasing rock-glacier discharge could be the cause of the increasing solute concentrations observed between the early and late ice-free season (Fig. 5, Table S1), due to the "concentration effect" caused by a probable inverse relationship between solute concentrations and rock-glacier discharge. This general basic pattern driven by air temperature was furtherly modified by the response of the rock-glacier outflow to liquid precipitation inputs. Indeed, Colombo et al., 2018b, Colombo et al., 2018c found that the main rock-glacier discharge contribution is associated with intense precipitation events. Concurrently with high discharges, electrical conductivity and solute peaks were observed (also during the ice-free season 2014, Fig. S2) leading to the assumption that the infiltration of rain water in the ice-sediment matrix might be able to increase rock-glacier ice melting, thus enhancing the export of mineralised waters. Therefore, the highest increase of solute concentrations observed during the middle ice-free season is attributed to higher precipitation in this period.

The absence of prevailing cryospheric features makes the NoPermafrost_pond basin less sensitive to the seasonal air temperature trend, which influences the thawing/melting processes and consequently solute concentrations. In fact, in this pond solute concentrations were stable or showed only slight

increases, if compared to the other ponds (Fig. 5, Table S1). For instance, the slight seasonal increases in EC at the NoPermafrost_pond is in agreement with the findings reported by Rogora et al. (2013) that analysed the water quality of 20 ponds in the Swiss Alps (2010–2011 period). These lakes were located at a mean elevation of 2130 m a.s.l., which allowed to reasonably exclude a significant contribution from cryospheric features.

4.2. Cryospheric features and chemical reactions

Reactions that donate H3O+ from the dissociation of organic and inorganic acids are crucial for chemical weathering in cryospheric-affected basins; H3O+ ions primarily derive from the dissociation of inorganic acids such as sulphuric, carbonic, or simple hydrolysis (Tranter et al., 2002; Stachnik et al., 2016). Dissolution of silicate or carbonate minerals is coupled to these reactions (Eqs. (1)–(6) in Table 3), which affect water chemistry by enriching it with ions resulting in altered ion ratios and different slopes and intercepts in linear regression equations (Table 3).

In the investigated area, all ponds except the NoPermafrost_pond show significant regression slopes ($0.77 < r < 0.99$, $p < 0.01$) for ion associations [Ca2+ + Mg2+ vs SO42−], [HCO3− vs SO42−], and [Ca2+ + Mg2+ vs HCO3−] (Fig. 7, Table S3). The significance of these relationships points out that processes responsible for donating H3O+ were more intensive in presence of cryospheric features like glacier, permafrost, and rock glacier. These regressions can be also attributed to other factors such as a progressive change in discharge during the ice-free season (as supposed above), that could generate dilution or concentrations of waters, resulting in significant relationships among major ions (Lamb et al., 1995). In this regard, Tranter et al. (2002) affirmed that it is probable that both hydrologic and chemical controls exist under cryospheric conditions.

4.2.1. Permafrost and glacier

4.2.1.1. Middle and late ice-free season

The lithology of the Glacier_pond and Permafrost_pond basins is prevalently siliceous. The slopes of [Ca2+ + Mg2+ vs SO42−] and [HCO3− vs SO42−] are close to the theoretical slopes of sulphide oxidation coupled to silicate dissolution (SDSO, Eq. (4) in Table 3) and far from the slopes for carbonation of silicate (SDC, Eq. (2)) (Fig. 7). Table S3 shows slopes of 0.96 and 1.0 for the regression [Ca2+ + Mg2+ vs SO42−] and 0.20 and 0.25 for the regression [HCO3− vs SO42−] for Glacier_pond

and Permafrost_pond, respectively. The comparison of these observed slopes with the theoretical values for SDSO (1 for [$Ca^{2+} + Mg^{2+}$ vs SO_4^{2-}] and 0 for [HCO_3^- vs SO_4^{2-}]) highlights a similarity. In addition, during the ice-free season, the mean S-ratio was 67 and 65% for Glacier_pond and Permafrost_pond, respectively. With S-ratio equal to 100%, weathering of silicate would be completely driven by sulphide oxidation and the slope of the regression [$Ca^{2+} + Mg^{2+}$ vs SO_4^{2-}] would be 0 (Eq. (4)). The observed [HCO_3^- vs SO_4^{2-}] slope equal to 0.20 and 0.25, and S-ratio equal to 67 and 65% suggest that under prevalent conditions of SDSO, other secondary reactions can occur, as discussed below.

4.2.1.2. Early ice-free season

During the early ice-free season S-ratio values were 43 and 51% at the Glacier_pond and Permafrost_pond, respectively (Fig. 6). These ratios increased during the ice free season (71% - Glacier_pond, 69% - Permafrost pond) (Fig. 6). Unfortunately, there are not enough data to perform regression calculations for each period of the ice-free season. However, the S-ratio value close to 50% at both ponds in the early ice-free season suggests predominant carbonate dissolution with sulphide oxidation (CDSO, Eq. 3). Albeit a lithological setting characterised mainly by acid-siliceous rocks, secondary carbonate-silicate rocks and basic rocks (i.e., calcite-rich rhodingitic gabbros) are also present in the basins (Fig. 2, Study area S1).

Previous studies (Tranter and Wadham, 2014; Stachnik et al., 2016) reported proportionally higher HCO_3^- concentrations in glacial meltwaters during the early ice-free season due to carbonate hydrolysis (CH, Eq. (5)) driven by simple contact between water and minerals. For instance, Tranter et al. (2002) suggested that, due to the water-saturated conditions of subglacial environments at the beginning of the ablation season, a decoupling between these environments and atmospheric CO_2 can occur. Thus, glacial meltwaters are initially involved in CH which does not require a proton source and is relatively rapid. Moreover, these authors observed that the theoretical solubility of calcite in distilled water, initially saturated with air, at 0 °C is ca. 250 μeq L^{-1} for Ca^{2+} and the [$Ca^{2+} + Mg^{2+}$ vs $HCO_3^- + CO_3^{2-}$] slope is close to the theoretical value of 1 (Eq. (5)). Therefore, in ions associations [$Ca^{2+} + Mg^{2+}$ vs SO_4^{2-}], an intercept lower than 250 μeq L^- indicates simple CH at the initial stage of water contact with subglacial sediments. In this study, intercepts ranging from 47 to 122 μeq L^{-1} were found for the Glacier_pond and Permafrost_pond, respectively (Table S3), suggesting that ($Ca^{2+} + Mg^{2+}$) concentrations derived by CH without additional H_3O^+ sources. However, the S-ratio

close to 50% suggests that simple hydrolysis was accompanied by additional processes at the initial stage of chemical weathering such as sulphide oxidation. Mean ($Ca^{2+} + Mg^{2+}$) concentrations in the early ice-free season were 83 and 294 μeq L^{-1} for the Glacier_pond and Permafrost_pond, respectively (Table S1). Subtracting these values from the intercepts, 36 and 172 μeq L^{-1} of ($Ca^{2+} + Mg^{2+}$) are obtained and could be due to SDSO, considering that SO_4^{2-} concentrations were 56 and 189 μeq L^{-1} at the Glacier_pond and Permafrost_pond, respectively (Table S1).

These observations indicate that in the early ice-free season CH coupled to SDSO gave an S-ratio close to 50%, while with the progression of the season, the increase of oxidative processes made SDSO the dominant reaction increasing the S-ratio. At the same time, CH remained rather constant during the ice-free season. This background reaction could have been further favoured by carbonic acid (CDC, Eq. 1), becoming more available as suggested by HCO_3^- increases (Fig. 5, Table S1).

4.2.1.3. Neutralisation of pH

CH and possible CDC with the progression of the ice-free season are supposed to be responsible for the observed pH increases (Fig. 5, Table S1) even if these reactions were not dominant. In general, a large amount of H_3O^+ results from pyrite oxidation, thus decreasing the pH. However, when sufficient carbonates are present, pH can be maintained neutral (Tranter et al., 2002). The alkalinisation processes observed in this study do not agree with acidification observed by some authors in other cryospheric settings (e.g., Salerno et al., 2016; Ilyashuk et al., 2018). These authors reported a decreasing pH due to sulphide oxidation in acid rock drainage (ARD) conditions. The present study evidences that acidification does not occur in presence of secondary amount of carbonate-rich rocks (i.e., even secondary amounts of carbonate rocks are able to buffer the pH against acidification derived by sulphide oxidation).

4.2.1.4. Sulphide oxidation

Regarding SO_4^{2-} increases, the rate of sulphide oxidation is controlled by the dissolved O_2 content, as well as the availability of reactive sulphides in sulphur-rich minerals (e.g., pyrite) (Williamson and Rimstidt, 1994; Tranter et al., 2002), that are present in the investigated area. Despite the declining dissolved O_2 concentrations as the reaction proceeds, microbial activity is likely to be the dominant influence on the rate of sulphide oxidation; indeed, laboratory experiments evidenced that microbially-

catalysed rates of oxidation can be at least two orders of magnitude greater than chemical rates (Sharp et al., 1999).

In the Glacier_pond, progressive increases in SO42− content can be attributed to chemical reactions, probably microbially mediated (Skidmore et al., 2005; Wadham et al., 2010), occurring in subglacial environments (Bottrell and Tranter, 2002; Stachnik et al., 2016). Here, mechanical comminution of bedrock by glacial ice can generate fresh mineral surfaces that are poised for chemical weathering (Tranter et al., 2002) and are capable to sustain chemotrophic microbial communities adapted to dark conditions in subglacial habitats, with biological pyrite oxidation that can drive mineral dissolution (Boyd et al., 2014; Harrold et al., 2016). The enrichment in SO42− is likely to be associated with delayed flow waters originating from distributed-type drainage beneath the glacier (Tranter et al., 1993; Wadham et al., 2010), indicating increasing residence time and rock/water interaction at the glacier bed (Cooper et al., 2002). Moreover, the abundance of freshly exposed mineral surfaces in recently deglaciated areas can favour the export of SO42− due to more rock exposed to air and enhanced mineral oxidation (e.g., Salerno et al., 2016). In fact, the Indren glacier has suffered an important reduction since the first decades of XX sec., loosing ca. 45% of the areal extension between 1955 and 2006 (from 1.68 to 0.92 km2) (CGI-CNR, 1961), similar to what occurred in other glaciated areas in the NW Italian Alps (Giaccone et al., 2015; Colombo et al., 2016b). It is also worth noting that SO42− content during the ice-free season 2014 reached a maximum of 194 μeq L−1 (Fig. S2) while in 2015 it peaked at 440 μeq L−1. Colombo et al. (2018c) found that the ice-free season in 2014 was colder than in 2015, with snow depletion occurring one month later. Thus, it is possible that enhanced weathering on freshly exposed mineral surfaces and a more developed subglacial hydrological system might have been responsible for greater inputs of sulphate into the pond.

In the Permafrost_pond, the increasing release of SO42− could be linked to enhanced oxidation processes in recently thawed zones, allowing migration of groundwater and O2 into the subsurface where they previously could not penetrate (Mast et al., 2011; Todd et al., 2012). This is corroborated by the observation at the temperature borehole of the progressive active layer thickening during the ice-free season 2015, reaching its maximum thickness in early October. Interestingly, the 30-m deep borehole data in 2014 and 2015 showed that the permafrost temperature on the southern slopes of the Permafrost_pond basin is close to 0 °C (Fig. 4). This evidence might indicate that permafrost could be thawing and subsurface ice could be melting, releasing latent heat.

4.2.1.5. Chemical weathering under glacier and permafrost conditions

It is important to highlight the similarity of the chemical reactions observed at the Glacier_pond and Permafrost_pond. Under prevalent acidic-silicate rocks and secondary calcite-rich rocks, the ice-free season displayed an initial simple CH coupled with SDSO. Along the ice-free season, SDSO became the dominant reaction donating H3O+, while CDC occurred only secondarily. However, the minor presence of carbonates allowed pH to increase; therefore, these environments are assumed to not play a significant role in atmospheric CO2 sequestration.

4.2.2. Rock glacier

In the RockGlacier_pond basin, metamorphic rocks with basic/ultrabasic composition and schistous texture (serpentinites, serpentineschists) are the dominant lithology (Fig. 2, Study area S1). Generally, serpentine minerals (Mg3Si2O5(OH)4) weather through exchange reactions between H3O+ and Mg2+ (Eq. (7)), analogous to Eqs. (2) and (4) in relation to the H3O+ donor, originating from the dissociation of sulphuric (Heikkinen and Räisänen, 2008) or carbonic (Kandji et al., 2017) acid. Despite its slow weathering rate, serpentine has been shown to be able to buffer the H3O+ although the neutralisation of acid is more likely to be provided by brucite (Mg(OH2)), considering that it is more reactive than serpentine (Bales and Morgan, 1985; Kandji et al., 2017). Brucite is abundant in the serpentinitic material composing the rock glacier. Generally, the weathering of these rocks give a high Mg-ratio (Kandji et al., 2017), as it was observed at the RockGlacier_pond (52%), while for the other basins the ratio was ca. 20% (Fig. 6). Furthermore, a decidedly lower S-ratio was found at the RockGlacier_pond (23%) in comparison to the mean values of the other basins (55%) (Fig. 6). This is due to relatively higher HCO3– and lower SO42− concentrations with respect to the other ponds (Fig. 5).

4.2.2.1. Early ice-free season

During the early ice-free season, the S-ratio at the RockGlacier_pond was 12% (Fig. 6), while HCO3– concentrations (235 μeq L−1) were an order of magnitude higher than SO42− concentrations (32 μeq L−1). Similar to the other ponds, HCO3– could have been released by CH; indeed, also in the RockGlacier_pond basin, secondary carbonate-silicate rocks are present. Given the 170 μeq L−1 intercept in the ion association [Ca2+ + Mg2+ vs SO42−], (Ca2+ + Mg2) concentrations probably originated by a simple CH without additional H3O+ sources. The mean (Ca2+ + Mg2+) concentration in the early ice-free season was 242 μeq L−1 (Table S1) and, subtracting this value from the intercept, a

value of 72 μeq L−1 of ($Ca^{2+} + Mg^{2+}$) is obtained, which requires a H_3O^+ source. This value could be due to the dissolution of brucite, considering that in this period the Mg-ratio of the RockGlacier_pond (46%) was higher with respect to the mean Mg-ratio of the Permafrost_pond and Glacier_pond (ca. 20%). H_3O^+ could have been released at an initial stage of both SDC and SDSO considering that SO_4^{2-} was 32 μeq L−1 and HCO_3^- was assumed to be 40 μeq L−1 (estimated subtracting 32 μeq L−1 of SO_4^{2-} from 72 μeq L−1 of ($Ca^{2+} + Mg^{2+}$)).

4.2.2.2. Middle and late ice-free season

With the progression of the ice-free season CH became a background process and the higher availably of CO_2 and O_2 provided by the contact with air and precipitation made H_3O^+ available. The [$Ca^{2+} + Mg^{2+}$ vs SO_4^{2-}] intercept is close to 3 (2.70), while [$Ca^{2+} + Mg^{2+}$ vs HCO_3^-] intercept is close to 2 (1.8), entailing that 2/3 of H_3O^+ were provided by carbonic acid (Eq. 2, SDC) and 1/3 of H_3O^+ was provided by sulphide oxidation (Eq. 4, SDSO).

4.2.2.3. Neutralisation of pH

Also at the RockGlacier_pond, pH increased during the ice-free season (Fig. 5, Table S1). As discussed above, CDC is responsible for maintaining neutral pH conditions; however, in this case pH increase was also favoured by SDC of Mg-bearing rocks (Kandji et al., 2017). As observed in other rock-glaciated settings (e.g., Ilyashuk et al., 2014, Ilyashuk et al., 2018; Salerno et al., 2016), ARD did not occur, while a less common neutral rock drainage (NRD) was observed due to the presence of carbonate-siliceous or Mg-bearing rocks (Heikkinen et al., 2009).

4.2.2.4. Chemical weathering under rock-glaciated conditions

Similarities exist among the ponds located in cryospheric settings. EC and major ions increased during the ice-free season. Processes that donate H_3O^+ were more intensive in presence of cryospheric features. Furthermore, the ice-free season began with a common CH. Main differences were observed due to the dominant lithology in the RockGlacier_pond basin, characterised by Mg-bearing rocks. With the progression of the ice-free season, the dissolution of Mg-bearing rocks occurred mainly with SDC, while SDSO was secondary. In this environment, pH was neutralised both by the presence of carbonates and by the carbonation of ultramafic rocks. Generally, it is possible to affirm that cryospheric features located in ultramafic settings can play a significant role in atmospheric CO_2

sequestration, favouring the carbonic to the sulphur acid, contrarily to what observed for acidic-silicate lithologies. Similar observations derive from ultramafic mine wastes where serpentines and brucite were observed to spontaneously react with CO2 (Kandji et al., 2017).

The presence of ultrabasic rocks in the RockGlacier_pond basin caused higher Ni concentrations in this pond than in the others (Fig. 5, Table 2). Generally, the mobility of Ni is higher at lower pH. In the RockGlacier_pond pH ranged from 7.2 to 7.7, and part of the dissolved Ni was found in water solution, while at higher pH (> 8) it would have been completely precipitated, as observed in ultramafic mine wastes (Kandji et al., 2017).

4.3. Biotic drivers on pond water quality

4.3.1. Nitrate

The lower NO_3^- concentrations in the NoPermafrost_pond and its reduced seasonal increase in comparison to the other ponds (Fig. 5, Table S1) could be attributed to the higher presence of soils and vegetation in the basin (Sickman et al., 2002) with the biological community playing a crucial role in limiting losses of nitrates (Kopácek et al., 2004; Balestrini et al., 2013), and lower slopes favouring nitrogen (N) retention (Kopácek et al., 1995; Kamenik et al., 2001). However, recent studies in different cryospheric settings reported higher mean NO_3^- concentrations and seasonal increases in systems fed by glacier/rock-glacier/permafrost ice meltwater in comparison to snow/groundwater-fed systems (e.g., Williams et al., 2007; Barnes et al., 2014).

Concerning the RockGlacier_pond basin, it is worth noting that, regardless of having the second most widespread relative soil distribution area among all basins (14.7%) after the NoPermafrost_pond basin (53.8%, Table 1), the highest seasonal NO_3^- value and increase (27 μeq L^{-1} and +508%, respectively, Table S1) were registered here during the middle ice-free season. During this period the rock glacier displayed the highest hydrological contribution to the pond (Colombo et al., 2018b). After this mid-season peak, NO_3^- strongly decreased in the late ice-free season, with concentrations approaching those observed in the NoPermafrost_pond. This occurrence indicates that the rock glacier is a fundamental factor in exporting N, and this evidence is even more striking if compared to a similar pond without a rock glacier (or other cryospheric features) in the catchment. Microbial communities adapted to extreme environments have been suggested as potential sources of the elevated NO_3^- in rock-glacier outflows (Williams et al., 2007). Similarly, the high NO_3^- values and increases at the

Permafrost_pond could be attributed to cryospheric factors. Indeed, Barnes et al. (2014) suggested that observed $NO3^-$ increase in high-elevated surface waters may be a result of meltwater flushing microbially-active sediments following permafrost degradation.

The Glacier_pond also showed relatively high values and increases in nitrate. Glacier runoff has been suggested to act as N source (Milner et al., 2017), concentrated in glacier ice from the atmosphere (Daly and Wania, 2005) or originating from microbial ecosystems on and beneath the ice (Wadham et al., 2016). However, the processes responsible for the increase in N export from glaciers are still object of debate, spanning from enhanced nitrification in subglacial environments (Wynn et al., 2007) to the release through abrasion of old organic N bound in rock (Boyd et al., 2011).

4.3.2. DOC and FI

DOC concentrations were very similar among the four ponds, without any clear seasonal trend (Fig. 5, Table S1), in agreement with the findings of Williams et al. (2007). In the Glacier_pond, the transient shifts in FI towards values <1.3 during the middle ice-free season suggest a potential component of terrestrially-derived DOC (McKnight et al., 2001; Lafrenière and Sharp, 2004; Barker et al., 2013). This is surprising since developed soils are absent in this basin. Thus, it is possible that the re-arrangement and flushing of the subglacial drainage system could be the cause, implying the existence of a source of terrestrially derived DOC in the subglacial environment (cf., Lafrenière and Sharp, 2004). However, further analyses are needed to improve our knowledge on the origin of DOC in the Indren Glacier meltwater. Differently, high FI values in the RockGlacier_pond during the middle ice-free season suggest a primarily aquatic-like microbial source, as already observed in a rock-glacier outflow in the Colorado Front Range (Williams et al., 2007). Interestingly, Mania et al. (2018) found microorganisms frequently associated with glacial and subglacial environments in the RockGlacier_pond sediments in early-September 2015, hypothesising a transient and localised, meltwater-driven microbial enrichment.

5. Conclusion

Permafrost degradation, rock-glacier thawing, and glacier retreat have been reported to impact chemical characteristics of surface waters across the globe. However, comprehensive investigations on the dynamics of high-elevation surface waters located in different cryospheric settings are uncommon and geographically scattered. In this study we show that chemical weathering is more intensive in presence of cryospheric conditions. Major ions strongly increase during the ice-free season in the ponds with cryospheric features in their basins due the progressive seasonal modifications of flowpaths and water sources, while no trends or slight increases occur in the pond without cryospheric features. Enhanced weathering of freshly exposed rocks in subglacial environment and recently deglaciated areas, and active layer thickness increase are probably the drivers of sulphide oxidation, which dominates in glacier and permafrost lying on acid rocks. Differently, carbonation dominates for the rock glacier lying on ultramafic rocks, with high Ni concentrations occurring in the RockGlacier_pond due to the dissolution of Mg-bearing rocks in the landform body. The neutralisation of pH takes place in all settings due to the presence of secondary carbonate lithology and ultramafic rocks. Among the biotic parameters, the highest concentrations and seasonal increases in nitrate occur in the ponds with cryospheric features in their basins probably due to limited presence of soils and vegetation together with higher slopes that limit N retention, and meltwater flushing microbially-active sediments. DOC and FI do not show strong differences and seasonal variations, although stronger variations in fluorescence index in glacier and rock-glacier ponds could indicate transient modifications of flowpaths and water sources in the glacier, and increasing contribution of internal ice from the rock glacier.

Although this study represents a temporal and geographic snapshot of the dynamics of cryospheric features-surface water interactions, it provides evidence of the importance of glaciers, permafrost, and rock glaciers in shaping the chemical dynamics of high-elevation ponds. Under the effects of climate change, the establishment of more frequent monitoring for water quality in high-elevation surface waters will provide greater statistical power to detect changes on longer time scales, overcoming the obvious limitations of short-term investigations performed in these remote areas.

Acknowledgments

Nicola Colombo and Franco Salerno equally contributed to this paper. We would like to thank Andrea Magnani, Elisa Giaccone, Emanuele Pintaldi, Davide Viglietti, Eleonora Conca and Marco Prati for

their help in data acquisition, fieldwork and laboratory activities. We give special thanks to Mark Williams and Holly Hughes (Department of Geography, University of Colorado, Boulder, USA), the family Beck-Peccoz, Consorzio di Miglioramento Fondiario di Gressoney (Aosta), and MonteRosa-ski. This research has been partially developed in the framework of the PRIN 2010-11 (funded project of the Italian Ministry for Education and Research) named “Response of morphoclimatic system dynamics to global changes and related geomorphological hazards” (coord. Prof. Carlo Baroni) and the European Regional Development Fund in Interreg Alpine Space project Links4Soils (ASP399): Caring for Soil-Where Our Roots Grow (http://www.alpine-space.eu/projects/links4soils).Finally, the editor and anonymous reviewers provided valuable feedback and input during the review of this manuscript. The datasets generated and/or analysed during the current study are available from the corresponding author on reasonable request.

References

Abbott, B.W., Larouche, J.R., Jones, J.B., Bowden, W.B., Balser, A.W., 2014.Elevated dis-solved organic carbon biodegradability from thawing and collapsing permafrost. J. Geophys. Res. Biogeosci. 119, 2049–2063.

Adrian, R., Reilly, C.M.O., Zagarese, H., Baines, S.B., Hessen, D.O., Keller, W., Livingstone, D.M., Sommaruga, R., Straile, D., Van Donk, E., Weyhenmeyer, G.A., Winder, M.,2009. Lakes as sentinels of climate change. Limnol. Oceanogr. 54 (6), 2283–2297.

Bales, R.C., Morgan, J.J., 1985.Dissolution kinetics of chrysotile at pH 7 to 10. Geochim. Cosmochim. Acta 49 (11), 2281–2288.

Balestrini, R., Arese, C., Freppaz, M., Buffagni, A., 2013.Catchment features controlling ni-trogen dynamics in running waters above the tree line (central Italian Alps). Hydrol. Earth Syst. Sci. 17, 989–1001.

Barker, J.D., Dubnick, A., Lyons, W.B., Chin, Y.P., 2013.Changes in dissolved organic matter(DOM)fluorescence in proglacial Antarctic streams. Arct. Antarct. Alp. Res. 45 (3),305–317.

Barnes, R.T., Williams, M.W., Parman, J.N., Hill, K., Caine, N., 2014.Thawing glacial and permafrost features contribute to nitrogen export from Green Lakes Valley, Colorado Front Range, USA. Biogeochemistry 117, 413–430.

Baron, J.S., Schmidt, T.M., Harman, M.D., 2009.Climate-induced changes in high-elevation stream nitrate dynamics. Glob. Chang. Biol. 15 (7), 1777–1789.

Beylich, A.A., Kolstrup, E., Linde, N., Pedersen, L.B., Thyrsted, T., Gintz, D., Dynesius, L., 2003. Assessment of chemical denudation rates using hydrological measurements, water chemistry analysis and electromagnetic geophysical data. Permafrost Periglac14, 387–397.

Bhatia, M.P., Das, S.B., Xu, L., Charette, M.A., Wadham, J.L., Kujawinski, E.B., 2013.Organiccarbon export from the Greenland ice sheet. Geochim. Cosmochim. Acta 109,329–344.

Boeckli, L., Brenning, A., Gruber, S., Noetzli, J., 2012a.Permafrost distribution in the European Alps: calculation and evaluation of an index map and summary statistics. Cryosphere 6, 807–820.

Boeckli, L., Brenning, A., Gruber, S., Noetzli, J., 2012b.A statistical approach to modelling permafrost distribution in the European Alps or similar mountain ranges. Cryosphere6, 125–140.

Bottrell, S.H., Tranter, M., 2002.Sulphide oxidation under partially anoxic conditions atthe bed of the Haut Glacier d'Arolla, Switzerland. Hydrol. Process. 16, 2363–2368.
Boyd, E.S., Lange, R.K., Mitchell, A.C., Havig, J.R., Hamilton, T.L., Lafrenière, M.J., Shock, E.L., Peters, J.W., Skidmore, M., 2011.Diversity, abundance, and potential activity of a ni-trifying and nitrate-reducing microbial assemblages in a subglacial ecosystem. Appl. Environ. Microbiol. 77, 4778–4787.
Boyd, E.S., Hamilton, T.L., Havig, J.R., Skidmore, M.L., Shock, E.L., 2014.Chemolithotrophicprimary production in a subglacial ecosystem. Appl. Environ. Microbiol. 80,6146–6153.
Brooks, R.R., 1987.Serpentine and its Vegetation. Dioscorides Press, Portland.
CGI-CNR, 1961.Catasto dei ghiacciai italiani. CGI (Comitato Glaciologico Italiano)-CNR(Consiglio Nazionale delle Ricerche) 2.
Colombo, N., Giaccone, E., Paro, L., Buffa, G., Fratianni, S., 2016a.Recent transition from glacial to periglacial environment in a high altitude alpine basin (Sabbione basin, north-western Italian Alps). Preliminary outcomes from a multidisciplinary approach. Geogr. Fis. Din. Quat. 39 (1), 21–36.
Colombo, N., Paro, L., Godone, D., Fratianni, S., 2016b.Geomorphology of the Hohsand basin (Western Italian Alps). J. Maps 12 (5), 975–978.Colombo, N., Salerno, F., Gruber, S., Freppaz, M., Williams, M.W., Fratianni, S., Giardino, M.,2018a.Review: impacts of permafrost degradation on inorganic chemistry of surface fresh water. Glob. Planet. Change 162, 69–83.
Colombo, N., Sambuelli, L., Comina, C., Colombero, C., Giardino, M., Gruber, S., Viviano, G.,Vittori Antisari, L., Salerno, F., 2018b.Mechanisms linking active rock glaciers and impounded surface water formation in high-mountain areas. Earth Surf. Process. Landf. 43 (2), 417–431.
Colombo, N., Gruber, S., Martin, M., Malandrino, M., Magnani, A., Godone, D., Freppaz, M., Fratianni, S., Salerno, F., 2018c.Rainfall as primary driver of discharge and solute ex-port from rock glaciers: the Col d'Olen Rock Glacier in the NW Italian Alps. Sci. Total Environ. 639, 316–330.
Cooper, R.J., Wadham, J.L., Tranter, M., Hodgkins, R., Peters, N., 2002.Groundwaterhydrochemistry in the active layer of the proglacial zone, Finsterwalderbreen, Sval-bard. J. Hydrol. 269, 208–223.
Crooke, W.M., Simpson, W.E., 1971.Determination of ammonium in Kjeldahl digests of crops by an automated procedure. J. Sci. Food Agric. 22, 9–10.
Daly, G.L., Wania, F., 2005.Organic contaminants in mountains. Environ. Sci. Technol. 39(2), 385–398.Drever, J.I., Zobrist, J., 1992.Chemical weathering of silicate rocks as a function of elevation in the southern Swiss Alps. Geochim. Cosmochim. Acta 56, 3209–3216.
Fegel, T.S., Baron, J.S., Fountain, A.G., Johnson, G.F., Hall, E.K., 2016.The differing biogeo-chemical and microbial signatures of glaciers and rock glaciers. J. Geophys. Res.Biogeosci. 121, 919–932.
Fortner, S.K., Mark, B.G., McKenzie, J.M., Bury, J., Trierweiler, A., Baraer, M., Burns, P.J., Mink, L., 2011.Elevated stream trace and minor element concentrations in the fore-land of receding tropical glaciers. Appl. Geochem. 26 (11), 1792–1801.899N.
Ge, S., McKenzie, J., Voss, C., Wu, Q., 2011. Exchange of groundwater and surface-water mediated by permafrost response to seasonal and long term air temperature variation. Geophys. Res. Lett. 38, L14402.https://doi.org/10.1029/2011GL047911.
Geiger, S.T., Daniels, J.M., Miller, S.N., Nicholas, J.W., 2014.Influence of rock glaciers on stream hydrology in theLaSal Mountains,Utah.Arct.Antarct.Alp.Res.46(3),645–658.
Giaccone, E., Colombo, N., Acquaotta, F., Paro, L., Fratianni, S., 2015.Climate variations in ahigh altitude Alpine basin and their effects on a glacial environment (Italian Western Alps). Atmósfera 28 (2), 117–128.
Goodrich, L.E., 1982.The influence of snow cover on the ground thermal regime. Can. Geotech. J. 19 (4), 421–432.

Gooseff, M.N., Van Horn, D., Sudman, Z., McKnight, D.M., Welch, K.A., Lyons, W.B., 2016.Stream biogeochemical and suspended sediment responses to permafrost degradation in stream banks in Taylor Valley, Antarctica. Biogeosciences 13, 1723–1732.
Gruber, S., Fleiner, R., Guegan, E., Panday, P., Schmid, M.-O., Stumm, D., Wester, P., Zhang,Y., Zhao, L., 2017.Review article: inferring permafrost and permafrost thaw in the mountains of the Hindu Kush Himalaya region. Cryosphere 11, 81–99.
Haeberli, W., Gruber, S., 2008.Mountain permafrost–research challenges for steep andcold terrain. Proceedings of the 9th International Permafrost Conference 597–605.
Hamerlík, L., Svitok, M., Novikmec, M., Očadlík, M., Bitušík, P., 2014.Local, among-site, and regional diversity patterns of benthic macroinvertebrates in high altitude waterbodies: do ponds differ from lakes? Hydrobiologia 723 (1), 41–52.
Harris, S., Pedersen, D., 1998.Thermal regimes beneath coarse blocky materials. Permafrost Periglac 9, 107–120.
Harris, C., Vonder Mühll, D., Isaksen, K., Haeberli, W., Sollid, J.L., King, L., Holmlund, P.,Dramis, F., Guglielmin, M., Palacios, D., 2003.Warming permafrost in Europeanmountains. Glob. Planet. Change 39 (3–4), 215–225.
Harris, H., Arenson, L.U., Christiansen, H.H., Etzelmüller, B., Frauenfelder, R., Gruber, S.,Haeberli, W., Hauck, C., Hoelzle, M., Humlum, O., Isaksen, K., Kääb, A., Kern-Lütschg,M.A., Lehning, M., Matsuoka, N., Murton, J., Noetzli, J., Phillips, M., Ross, N., Seppälä, M., Springman, S., Vonder Mühll, D., 2009. Permafrost and climate in Europe: monitoring and modelling thermal, geomorphological and geotechnical responses. EarthSci. Rev. 92, 117–171.
Harrold, Z.R., Skidmore, M.L., Hamilton, T.L., Desch, L., Amada, K., van Gelder, W., Glover,K., Roden, E.E., Boyd, E.S., 2016.Aerobic and anaerobic thiosulfate oxidation by a cold-adapted, subglacial chemoautotroph. Appl. Environ. Microbiol. 82, 1486–1495.
Heikkinen, P.M., Räisänen, M.L., 2008.Mineralogical and geochemical alteration of Hitura sulphide mine tailings with emphasis on nickel mobility and retention. J. Geochem.Explor. 97, 1–20.
Heikkinen, P.M., Räisänen, M.L., Johnson, R.H., 2009.Geochemical characterisation ofseepage and drainage water quality from two sulphide mine tailings impoundments: acid mine drainage versus neutral mine drainage. Mine Water Environ. 28 (1), 30–49.
Hock, R., 2003.Temperature index melt modeling in mountain areas. J. Hydrol. 282,104–115.
Hoelzle, M., 1992.Permafrost occurrence from BTS measurements and climatic parame-ters in the Eastern Swiss Alps. Permafrost Periglac 3, 143–147.
Hood, E., Fellman, J., Spencer, R.G.M., Hernes, P.J., Edwards, R., D'Amore, D., Scott, D., 2009.Glaciers as a source of ancient and labile organic matter to the marine environment. Nature 462, 1044–1047.
Hood, E., Battin, T.J., Fellman, J., O'Neel, S., Spencer, R.G.M., 2015.Storage and release of organic carbon from glaciers and ice sheets. Nat. Geosci. 8 (2), 91–96.
Ilyashuk, B.P., Ilyashuk, E.A., Psenner, R., Tessadri, R., Koinig, K.A., 2014.Rock glacier out-flows may adversely affect lakes: lessons from the past and present of two neighbor-ing water bodies in a crystalline-rock watershed. Environ. Sci. Technol. 48,6192–6200.
Ilyashuk, B.P., Ilyashuk, E.A., Psenner, R., Tessadri, R., Koinig, K.A., 2018.Rock glaciers in crystalline catchments: hidden permafrost-related threats to alpine headwater lakes. Glob. Chang. Biol. 24 (4), 1548–1562.
Ishikawa, M., 2003.Thermal regimes at the snow-ground interface and their implications for permafrost investigation. Geomorphology 52, 105–120.Julián, A., Chueca, J., 2007.Permafrost distribution from BTS measurements (Sierra de Telera, central Pyrenees, Spain): assessing the importance of solar radiation in amid-elevation shaded mountainous area. Permafrost Periglac 18, 137–149.

Kamenik, C., Schmidt, R., Kum, G., Psenner, R., 2001.The influence of catchment characteristics on the water chemistry of mountain lakes. Arct. Antarct. Alp. Res. 33 (4), 404–409.
Kandji, E.H.B., Plante, B., Bussière, B., Beaudoin, G., Dupont, P.P., 2017.Kinetic testing to evaluate the mineral carbonation and metal leaching potential of ultramafic tailings: case study of the Dumont nickel project, Amos, Québec. Appl. Geochem. 84, 262–276.
Keller, K., Blum, J.D., Kling, G.W., 2010.Stream geochemistry as an indicator of increasing permafrost thaw depth in an arctic watershed. Chem. Geol. 273 (1–2), 76–81.
Kopácek, J., Prochazkova, L., Stuchlfk, E., Plazka, P., 1995.The nitrogen-phosphorus relationship in mountain lakes: influence of atmospheric input, watershed, and pH. Limnol. Oceanogr. 40, 930–937.
Kopácek, J., Kana, J., Santruckova, H., Picek, T., Stuchlik, E., 2004.Chemical and biochemical characteristics of alpine soils in the Tatra Mountains and their correlation with lake water quality. Water Air Soil Pollut. 153, 307–327.
Krainer, K., Mostler, W., Spötl, C., 2007.Discharge from active rock glaciers, Austrian Alps: a stable isotope approach. Austrian J. Earth Sci. 100, 102–112.
Lafrenière, M.J., Sharp, M.J., 2004.The concentration and fluorescence of dissolved organic carbon (DOC) in glacial and nonglacial catchments: interpreting hydrological flowrouting and DOC sources. Arct. Antarct. Alp. Res. 36, 156–165.
Lamb, H.R., Tranter, M., Brown, G.H., Hubbard, B.P., Sharp, M.J., Smart, C.C., Willis, I.C., Nielsen, M.K., 1995.The composition of subglacial meltwaters sampled from bore-holes at the Haut Glacier d'Arolla. IAHS Publ. 138, 395–405.
Leonoris, C., Freppaz, M., Caimi, A., Filippa, G., Dal Piaz, G.V., Dal Piaz, G., Schiavo, A., 2009. Cimalegna Geologic and Pedologic field trip. Parco Naturale Alta Valsesia, RegionePiemonte.
Levy, J.S., Fountain, A.G., Gooseff, M.N., Welch, K.A., Lyons, W.B., 2011.Water tracks and permafrost in Taylor Valley, Antarctica: extensive and shallow groundwater connectivity in a cold desert ecosystem. Geol. Soc. Am. Bull. 123 (11−12), 2295–2311.
Maggioni, M., Freppaz, M., Piccini, P., Williams, M.W., Zanini, E., 2009.Snow cover effects on glacier ice surface temperature. Arct. Antarct. Alp. Res. 41 (3), 323–329.
Mania, I., Gorra, R., Colombo, N., Freppaz, M., Martin, M., Anesio, A.M., 2018. Prokaryotic diversity and distribution in different habitats of an alpine rock glacier-pond system. Environ. Microbiol. https://doi.org/10.1007/s00248-018-1272-3.
Marchetto, A., Mosello, R., Psenner, R., Bendetta, G., Boggero, A., Tait, D., Tartari, G.A., 1995. Factors affecting water chemistry of alpine lakes. Aquat. Sci. 57, 81–89.
Mast, M.A., Turk, J.T., Clow, D.W., Campbell, D.H., 2011.Response of lake chemistry to changes in atmospheric deposition and climate in three high-elevation wilderness areas of Colorado. Biogeochemistry 103 (1–3), 27–43.
McKnight, D.M., Boyer, E.W., Westerhoff, P.K., Doran, P.T., Kulbe, T., Andersen, D.T., 2001. Spectrofluorometric characterization of dissolved organic matter for indication of precursor organic material and aromaticity. Limnol. Oceanogr. 46, 38–48.
Milner, A.M., Khamis, K., Battin, T.J., Brittain, J.E., Barrand, N.E., Füreder, L., Cauvy-Fraunié,S., Gíslason, G.M., Jacobsen, D., Hannah, D.M., Hodson, A.J., Hood, E., Lencioni, V.,Ólafsson, J.S., Robinson, C.T., Tranter, M., Brown, L.E., 2017. Glacier shrinkage driving global changes in downstream systems. Proc. Natl. Acad. Sci. U. S. A. 114 (37),9770–9778.
Paro, L., Guglielmin, M., 2013.Sintesi e primi risultati delle attività di ARPA Piemonte su ambiente periglaciale e permafrost nelle Alpi piemontesi. Neve e Valanghe 80, 50–59.
PERMOS, 2016. Permafrost in Switzerland 2010/2011 to 2013/2014. In: Noetzli, J., Luethi,R., Staub, B. (Eds.), Glaciological Report (Permafrost) No. 12–15 of the Cryospheric Commission of the Swiss Academy of Sciences.

Polesello, S., Tartari, G., Giacomotti, P., Mosello, R., Cavalli, S., 2006. Determination of total dissolved inorganic carbon in freshwaters by reagent-free ion chromatography. J. Chromatogr. A 1118, 56–61.
R Core Team, 2019. R: A Language and Environment for Statistical Computing. R Foundation for Statistical Computing, Vienna, Austria URL.https://www.R-project.org/,Accessed date: 24 April 2019.
Roberts, K.E., Lamoureux, S.F., Kyser, T.K., Muir, D.C.G., Lafrenière, M.J., Iqaluk, D.,Pieńkowski, A.J., Normandeau, A., 2017. Climate and permafrost effects on the chemistry and ecosystems of high Arctic lakes. Sci. Rep. 7, 13292.https://doi.org/10.1038/s41598-017-13658-9.
Rogora, M., Colombo, L., Lepori, F., Marchetto, A., Steingruber, S., Tornimbeni, O., 2013.Thirty years of chemical changes in alpine acid-sensitive lakes in the Alps. Water Air Soil Pollut. 224, 1746. https://doi.org/10.1007/s11270-013-1746-3.
Salerno, F., Gambelli, S., Viviano, G., Thakuri, S., Guyennon, N., D'Agata, C., Diolaiuti, G.,Smiraglia, C., Stefani, F., Bocchiola, D., Tartari, G., 2014.High alpine ponds shift upwards as average temperatures increase: a case study of the Ortles-Cevedale mountain group(Southern Alps, Italy) over the last 50 years. Glob. Planet. Change 120, 81–91.
Salerno, F., Rogora, M., Balestrini, R., Lami, A., Tartari, G.A., Thakuri, S., Godone, D., Freppaz,M., Tartari, G., 2016.Glacier melting increases the solute concentrations of Himalayan glacial lakes. Environ. Sci. Technol. 50 (17), 9150–9160.
Seppi, R., Zanoner, T., Carton, A., Bondesan, A., Francese, R., Carturan, L., Zumiani, M.,Giorgi, M., Ninfo, A., 2015.Current transition from glacial to periglacial processes in the Dolomites (South-Eastern Alps). Geomorphology 228, 71–86.
Sharp, M., Parkes, J., Cragg, B., Fairchild, I.J., Lamb, H., Tranter, M., 1999.Widespread bacterial populations at glacier beds and their relationship to rock weathering and car-bon cycling. Geology 27, 107–110.
Sickman, O.J., Melack, J.M., Stoddard, J.L., 2002.Regional analysis of inorganic yield and re-tention in high-elevation ecosystems of the Sierra Nevada and Rocky Mountains. Bio-geochemistry 57–58, 341–374.
Skidmore, M., Anderson, S.P., Sharp, M.J., Foght, J., Lanoil, B.D., 2005. Comparison of micro-bial community compositions of two subglacial environments reveals a possible role for microbes in chemical weathering processes. Appl. Environ. Microbiol. 71,6986–6997.
Slemmons, K.E., Saros, J.E., Simon, K., 2013.The influence of glacial meltwater on alpine aquatic ecosystems: a review. Environmental Sciences: Processes and Impacts 15,1794–1806.
Stachnik, L., Majchrowska, E., Yde, J.C., Nawrot, A.P., Cichała-Kamrowska, K., Ignatiuk, D., Piechota, A., 2016. Chemical denudation and the role of sulfide oxidation at Werenskioldbreen, Svalbard. J. Hydrol. 538, 177–193.
Szopińska, M., Szumińska, D., Polkowska, Z., Machowiak, K., Lehmann, S., Chmiel, S., 2016.The chemistry of river-lake systems in the context of permafrost occurrence (Mongolia, Valley of the Lakes). Part I. Analysis of ion and trace metal concentrations. Sediment. Geol. 340, 74–83.
Szumińska, D., Szopińska, M., Lehmann-Konera, S., Franczak,Ł., Kociuba, W., Chmiel, S., Kalinowski, P., Polkowska,Ż., 2018. Water chemistry of tundra lakes in the periglacial zone of the Bellsund Fiord (Svalbard) in the summer of 2013. Sci. Total Environ. 624,1669–1679.
Thies, H., Nickus, U., Tolotti, M., Tessadri, R., Krainer, K., 2013.Evidence of rock glacier melt impacts on water chemistry and diatoms in high mountain streams. Cold Reg. Sci. Technol. 96, 77–85.
Todd, A.S., Manning, A.-H., Verplanck, P.L., Crouch, C., McKnight, D.M., Dunham, R., 2012. Climate-change-driven deterioration of water quality in a mineralized watershed. Environ. Sci. Technol. 46 (17), 9324–9332.

Toohey, R.C., Herman-Mercer, N.M., Schuster, P.F., Mutter, E., Koch, J.C., 2016.Multidecadal increases in the Yukon River Basin of chemical fluxes as indicators of changing flowpaths, groundwater, and permafrost. Geophys. Res. Lett. 43 (12),120–212 (130).
Tranter, M., 2006.Glacial chemical weathering, runoff composition and solute fluxes. In: Knight, P.G. (Ed.), Glacier Science and Environmental Change. Wiley-Blackwell, pp. 71–75
Tranter, M., Wadham, J.L., 2014.Geochemical weathering in glacial and proglacial envi-ronments. In: Holland, D., Turekian, K.K. (Eds.), Treatise on Geochemistry, Second edition vol. 7. Elsevier Science, pp. 157–173.
Tranter, M., Brown, G.H., Raiswell, R., Sharp, M.J., Gurnell, A., 1993.A conceptual model of solute acquisition by Alpine glacial meltwaters. J. Glaciol. 39, 573–581.
Tranter, M., Sharp, M.J., Lamb, H.R., Brown, G.H., Hubbard, B.P., Willis, I.C., 2002.Geochem-ical weathering at the bed of Haut Glacier d'Arolla. Switzerland - a new model. Hydrol. Process. 16, 959–993.
Wadham,J.L.,Tranter,M.,Skidmore,M.,Hodson,A.D.,Priscu,J.,Lyons,W.B.,Sharp,M.,Wynn,P., Jackson, M.., 2010. Biogeochemical weathering under ice: size matter. Glob. Biogeochem. Cycles 24, GB 3025. doi.org/https://doi.org/10.1029/2009GB003688.
Wadham, J.L., Hawkings, J., Telling, J., Chandler, D., Alcock, J., O'Donnell, E., Kaur, P.,Bagshaw, E., Tranter, M., Tedstone, A., Nienow, P., 2016. Sources, cycling and export of nitrogen on the Greenland ice sheet. Biogeosciences 13, 6339–6352.
Williams, M.W., Melack, J.M., 1991.Solute chemistry of snowmelt and runoff in an Alpine Basin, Sierra Nevada. Water Resour. Res. 27 (7), 1575–1588.
Williams, M.W., Knauf, M., Caine, N., Liu, F., Verplanck, P.L., 2006.Geochemistry and source water of rock glacier outflow, Colorado Front Range. Permafrost Periglac 17,13–33.
Williams, M.W., Knauf, M., Cory, R., Caine, N., Liu, N., 2007.Nitrate content and potential microbial signature of rock glacier outflow, Colorado Front Range. Earth Surf. Process. Landf. 32, 1032–1047.
Williamson, M.A., Rimstidt, J.D., 1994.The kinetics and electrochemical rate-determining step of aqueous pyrite oxidation. Geochim. Cosmochim. Acta 58 (24), 5443–5454.
Wynn, P.M., Hodson, A.J., Heaton, T.H.E., Chenery, S.R., 2007.Nitrate production beneath a high arctic glacier, Svalbard. Chem. Geol. 244, 88–102.
Yde, J.C., 2011.Hydrochemical characteristics of snow, ice, and glaciers. In: Singh, V.P., Singh, P., Haritashya, U.K. (Eds.), Encyclopedia of Snow, Ice and Glaciers. Springer, pp. 530–533.
Zemp, M., Frey, H., Gärtner-Roer, I., Nussbaumer, S.U., Hoelzle, M., Paul, F., et al., 2015. Historically unprecedented global glacier decline in the early 21st century. J. Glaciol. 61(228), 745–762.
Zhang, T., Osterkamp, T.E., Stamnes, K., 1997.Effects of climate on the active layer and permafrost on the North Slope of Alaska, USA. Permafrost Periglac. 8, 45–67

Tables

Table 1. Morphometric, cryospheric and land cover characteristics of the investigated pond basins. Where reported, the range is in brackets. Morphometric characteristics for the Glacier_pond and RockGlacier_pond basins were analysed using a 2mx2m-cell digital elevation model-DEM (produced by Regione Valle d'Aosta) while for the Permafrost_pond and NoPermafrost_pond basins a 5mx5m-cell DEM was used (produced by Regione Piemonte). The land cover characteristics of the basins were mapped by photointerpretation of digital orthoimages (years 2006 and 2012) (source: www.pcn.minambiente.it).

Feature	Glacier_pond	Permafrost_pond	RockGlacier_pond	NoPermafrost_pond
Pond elevation (m a.s.l.)	3083	2900	2722	2800
Pond area (m^2)	3230	2405	1600	2590
Basin area (km^2)	1.43	0.05	0.21	0.04
Basin mean elevation (m a.s.l.)	3503 (3083–4166)	2932 (2900–3020)	2830 (2722–3022)	2829 (2800–2865)
Basin mean slope (°)	29 (0–84)	26 (0–84)	21 (0–48)	15 (0–38)
Basin mean aspect (°)	191	105	217	140
Basin mean Permafrost Index-PI (0–1)	0.99 (0.97–1)	0.95 (0.91–1)	0.73 (0.14–0.97)	0.83 (0.76–0.89)
Basin land cover	Bedrock: 32% Coarse sediment: 3.7% Soil: 0% Glacier: 64.1% Pond: 0.2%	Bedrock: 23.4% Coarse sediment: 62.4% Soil: 9.5% Pond: 4.7%	Bedrock: 26% Coarse sediment: 58.5% Soil: 14.7% Pond: 0.8%	Bedrock: 35.3% Coarse sediment: 5% Soil: 53.8% Pond: 5.9%

Table 2. – Statistical summary of water chemistry monitored for ponds, snow, and rain in 2015. For each variable, median, mean, and standard deviation are reported. Solute, pH, electrical conductivity (EC), dissolved organic carbon (DOC) concentrations, and fluorescence index (FI) are reported. FI was not measured in snow and rain. Where present, limit of detection (LOD) NO2− > 0.5 μeq L−1, PO43− > 4 μeq L−1, HCO3− > 4.2 μeq L−1, Mg2+ > 0.8 μeq L−1.

Parameter	Glacier_pond	Permafrost_pond	RockGlacier_pond	NoPermafrost_pond	Snow	Rain
pH	6.9|7|0.3	7.4|7.4|0.2	7.5|7.5|0.2	7.2|7.2|0.1	5.6|5.6|0.2	5.8|6|0.4
EC (μS cm^{-1}, 20 °C)	44|38|19	92|84|30	61|60|23	36|36|3	4|4|1	6|7|4
Cl^- (μeq L^{-1})	2|2|2	5|5|2	3|3|1	2|3|4	5|5|2	2|3|1
SO_4^{2-} (μeq L^{-1})	251|202|137	547|455|208	124|112|59	106|104|16	6|6|2	6|8|7
NO_3^- (μeq L^{-1})	14|14|8	16|14|8	6|10|9	3|4|3	4|5|2	12|10|6
NO_2^- (μeq L^{-1})	<LOD	<LOD	<LOD	<LOD	<LOD	<LOD
PO_4^{3-} (μeq L^{-1})	<LOD	<LOD	<LOD	<LOD	<LOD	<LOD
HCO_3^- (μeq L^{-1})	85|99|31	243|245|58	330|342|71	178|172|31	<LOD	<LOD
Ca^{2+} (μeq L^{-1})	219|186|103	530|470|166	230|224|70	211|209|18	9|9|3	7|5|2
Mg^{2+} (μeq L^{-1})	49|54|34	130|107|49	271|246|96	43|45|8	<DL	<DL
K^+ (μeq L^{-1})	8|8|5	29|28|7	7|10|5	20|20|4	4|4|3	1|1|1
Na^+ (μeq L^{-1})	4|6|4	22|20|5	5|5|2	10|10|3	5|6|3	2|3|2
NH_4^+ (μeq L^{-1})	2|2|0.9	1|0.8|0.6	0.4|0.7|0.7	0.5|0.6|0.8	2|3|1	15|15|6
Si (μmol L^{-1})	17|16|8	26|26|9	18|22|8	30|30|7	3|4|3	1|1|0.3
Ni (nmol L^{-1})	22|22|7	41|42|16	280|340|196	21|21|6	3|7|9	11|11|1
Mn (nmol L^{-1})	30|39|25	3|6|9	23|67|72	6|5|3	8|12|11	16|16|2
Co (nmol L^{-1})	1|1.3|0.8	0.7|0.8|0.3	1.2|1.4|1	0.4|0.5|0.1	0.2|0.3|0.2	0.3|0.3|0.1
DOC (mg L^{-1})	1.1|1.2|0.4	1.4|1.4|0.3	1.6|1.5|0.4	1.5|1.3|0.3	0.8|0.8|0.1	1.3|1.3|0.3
FI	1.4|1.4|0.3|	1.6|1.6|0.1	1.6|1.6|0.2	1.5|1.5|0.1	/	/

Table 3. Main reactions of chemical weathering processes in cryospheric basins, theoretical slopes, and S-ratio (modified from Tranter et al., 2002 and Stachnik et al., 2016).

Eq.	Reaction	Formula	Theoretical slopes		S-ratio
			$(Ca^{2+} + Mg^{2+})$ vs HCO_3^-	$(Ca^{2+} + Mg^{2+})$ vs SO_4^{2-}	
(1)	Carbonate Dissolution with Carbonic acid (CDC)	$Ca_{1-x}(Mg_x)CO_3(s) + CO_2(aq) + H_2O(aq) \leftrightarrows (1-x)Ca^{2+}(aq) + xMg^{2+}(aq) + 2HCO_3^-(aq)$	1	0	0
(2)	Silicate Dissolution with Carbonic acid (SDC)	$CaAl_2Si_2O_8(s) + 2CO_2(aq) + 2H_2O(aq) \leftrightarrows Ca^{2+}(aq) + 2HCO_3^-(aq) + Al_2Si_2O_8(s)$	1	0	0
(3)	Carbonate Dissolution with Sulphide Oxidation (CDSO)	$4FeS_2(s) + 16Ca_{1-x}(Mg_x)CO_3(S) + 15O_2(aq) + 14H_2O(aq) \leftrightarrows 16(1-x)Ca^{2+}(aq) + 16xMg^{2+}(aq) + 16HCO_3^-(aq) + 8SO_4^{2-}(aq) + 4Fe(OH)_3(s)$	2	2	0.5
(4)	Silicate Dissolution with Sulphide Oxidation (SDSO)	$2FeS_2(s) + 4CaAl_2Si_2O_8(s) + 2O_2(aq) + 22H_2O(aq) \leftrightarrows 4Ca^{2+}(aq) + 4SO_4^{2-}(aq) + 2Al_4Si_4O_{10}(OH)_8(s) + 2Fe(OH)_3(s)$	0	1	1
(5)	Carbonate Hydrolysis (CH)	$Ca_{1-x}(Mg_x)CO_3(s) + H_2O(l) \leftrightarrows (1-x)Ca^{2+}(aq) + xMg^{2+}(aq) + HCO_3^-(aq) + OH^-(aq)$	1	0	0
(6)	Silicate Hydrolysis (SH)	$CaAl_2Si_2O_8(s) + 8H_2O(l) \leftrightarrows 2H_4SiO_4(aq) + Ca^{2+}(aq) + 2OH^-(aq) + 2Al(OH)_3(s)$	0	0	0
(7)	Mg-bearing silicate	$Mg_3Si_2O_5(OH)_4(s) + 6H^+(aq) \leftrightarrows 3Mg^{2+}(aq) + 2H_4SiO_4(aq) + H_2O(aq)$	Analogous to Eq. 2, 4, 6		

Figures

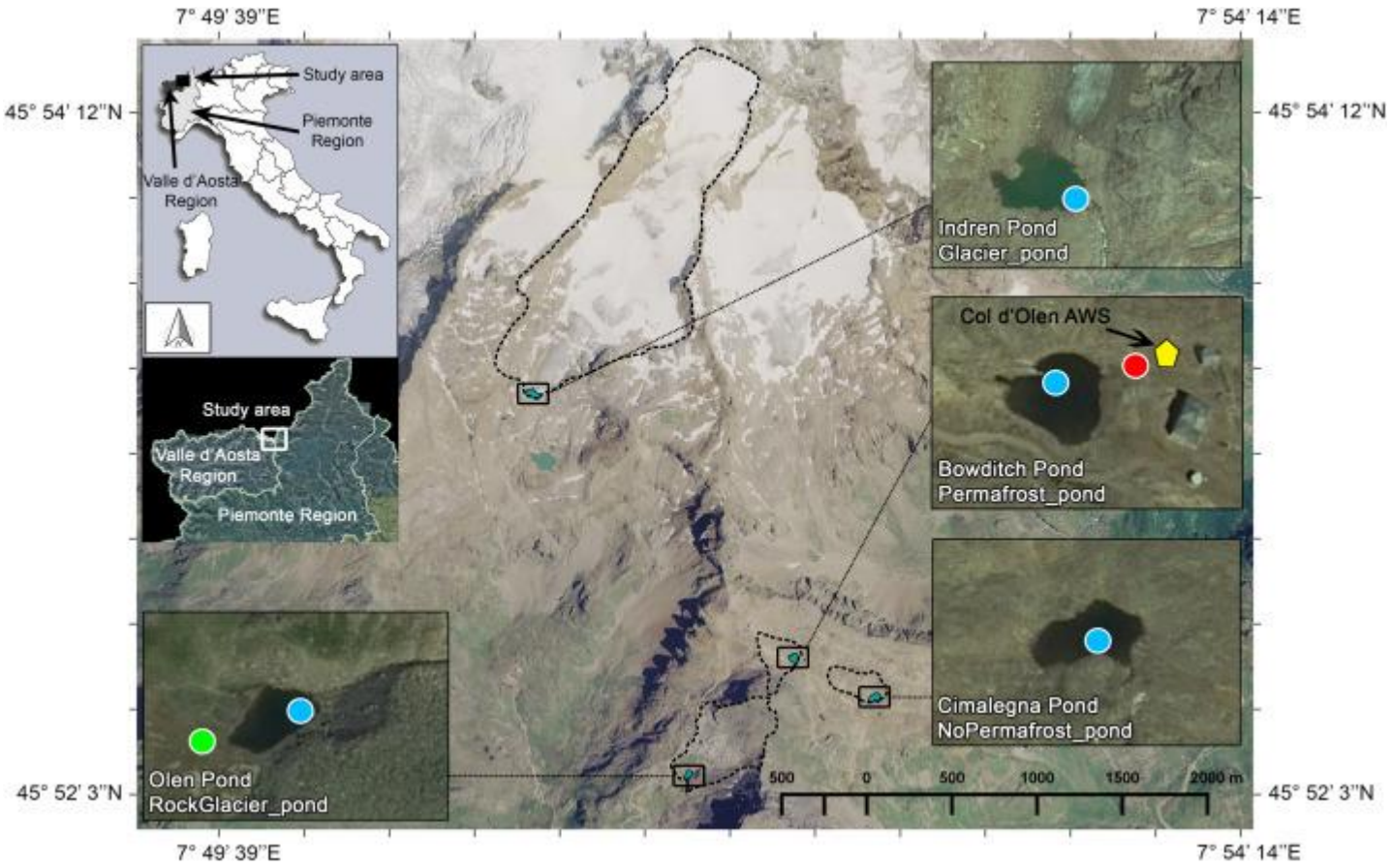

Fig. 1. Location of the study area in Italy and in the NW Italian Alps (www.pcn.minambiente.it), aerial overview of the study area (orthoimage year 2006), and details of each pond (Google Earth, Image©2018 DigitalGlobe). Black dashed lines indicate the hydrographic basin borders, pale blue circles refer to the water chemistry sampling locations, the red circle refers to the snow-profile site, and the green circle refers to the rain collector location. The yellow pentagon indicates the Col d'Olen AWS.

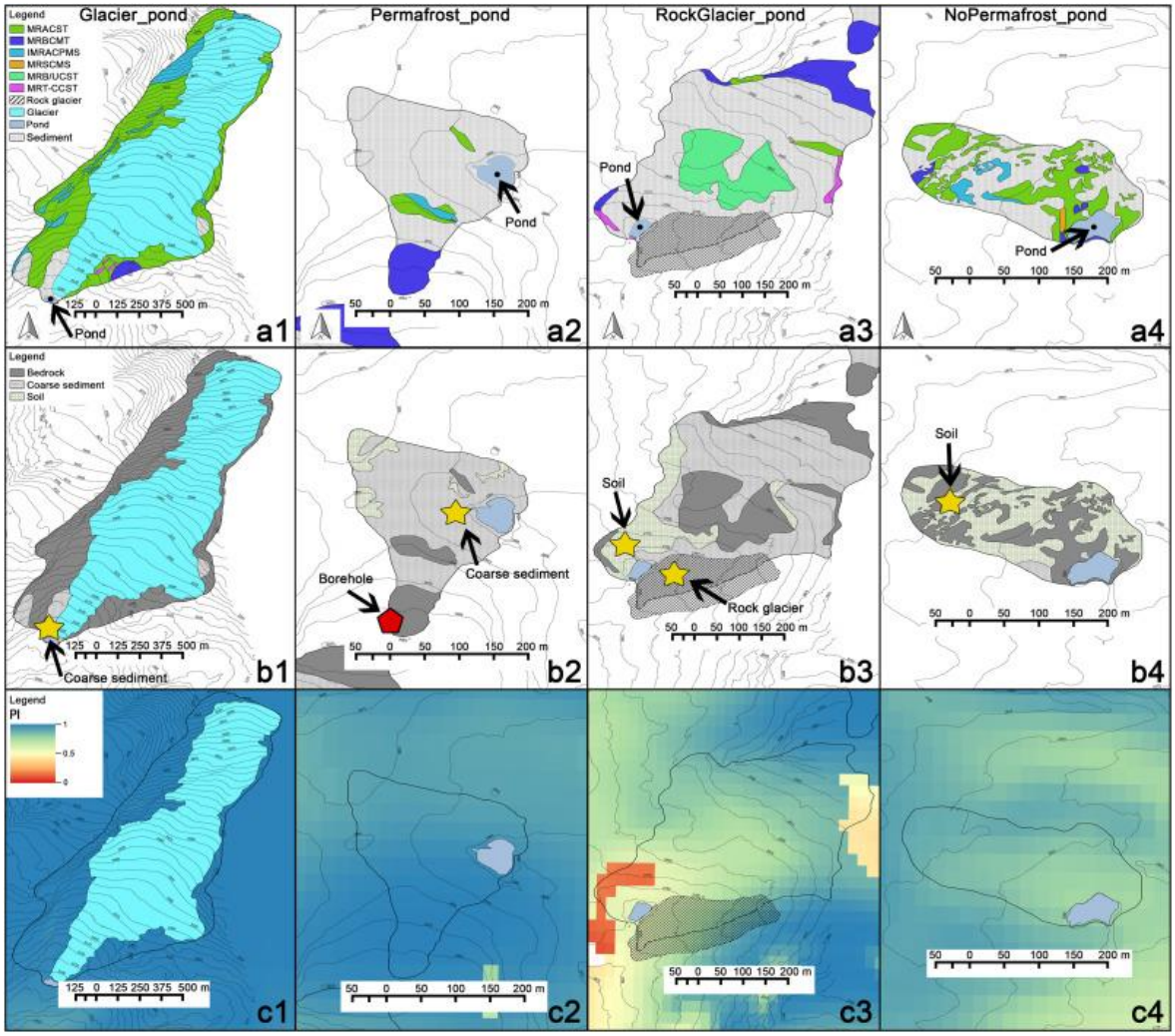

Fig. 2. Lithological (a), land cover (b), and potential permafrost distribution (c) maps of the Glacier_pond (1), Permafrost_pond (2), RockGlacier_pond (3), and NoPermafrost_pond (4) basins. (a1–a4) Codes for lithology identification are: MRACST – Metamorphic rocks with acid composition and schistous texture (micaschists, paraschists, polimetamorphic schists with minor migmatite bodies); MRBCMT – Metamorphic rocks with basic composition and massive texture (amphibolites, metabasites, prasinites, rhodingitic metagabbros); IMRACPMS – Intrusive and metamorphic rocks, with acid composition, prevalently with massive structure (gneiss, leucochratic gneiss, metagranites); MRSCMS – Metamorphic rocks with silica composition and massive structure (quartzites); MRB/UCST – Metamorphic rocks with basic/ultrabasic composition and schistous texture (serpentinites, serpentineschists); MRT-CCST – Metamorphic rocks with a terrigenous-carbonatic composition and schistous texture (calcschists). (b1–b4) The yellow stars indicate the ground surface temperature (GST) measurement sites. The red pentagon in b2 indicates the 30-m borehole location. (c1–c4) Alpine Permafrost Index Map (APIM) of the study area (Boeckli et al., 2012a). Permafrost Index (PI) 0 (permafrost only in very favourable conditions), 0.5 (permafrost mostly in cold conditions), and 1 (permafrost in nearly all conditions).

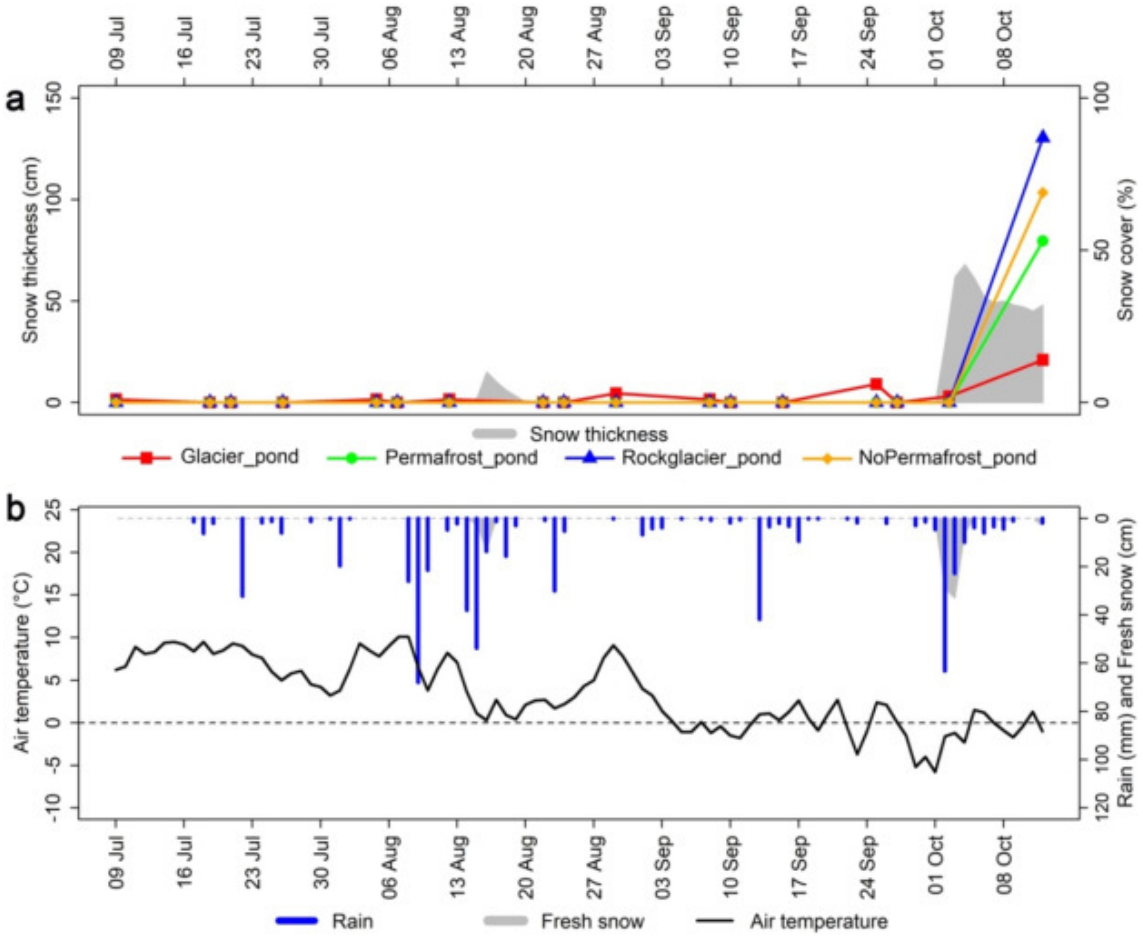

Fig. 3. (a) Snow thickness (grey polygons) and percentage of each pond basin covered by snow from Landsat data (lines, punctual symbols represent analysed images for each basin, those with cloud cover were excluded) during the ice-free season 2015. (b) Daily rain (blue histograms), fresh snow (grey polygons), and mean air temperature (black line).

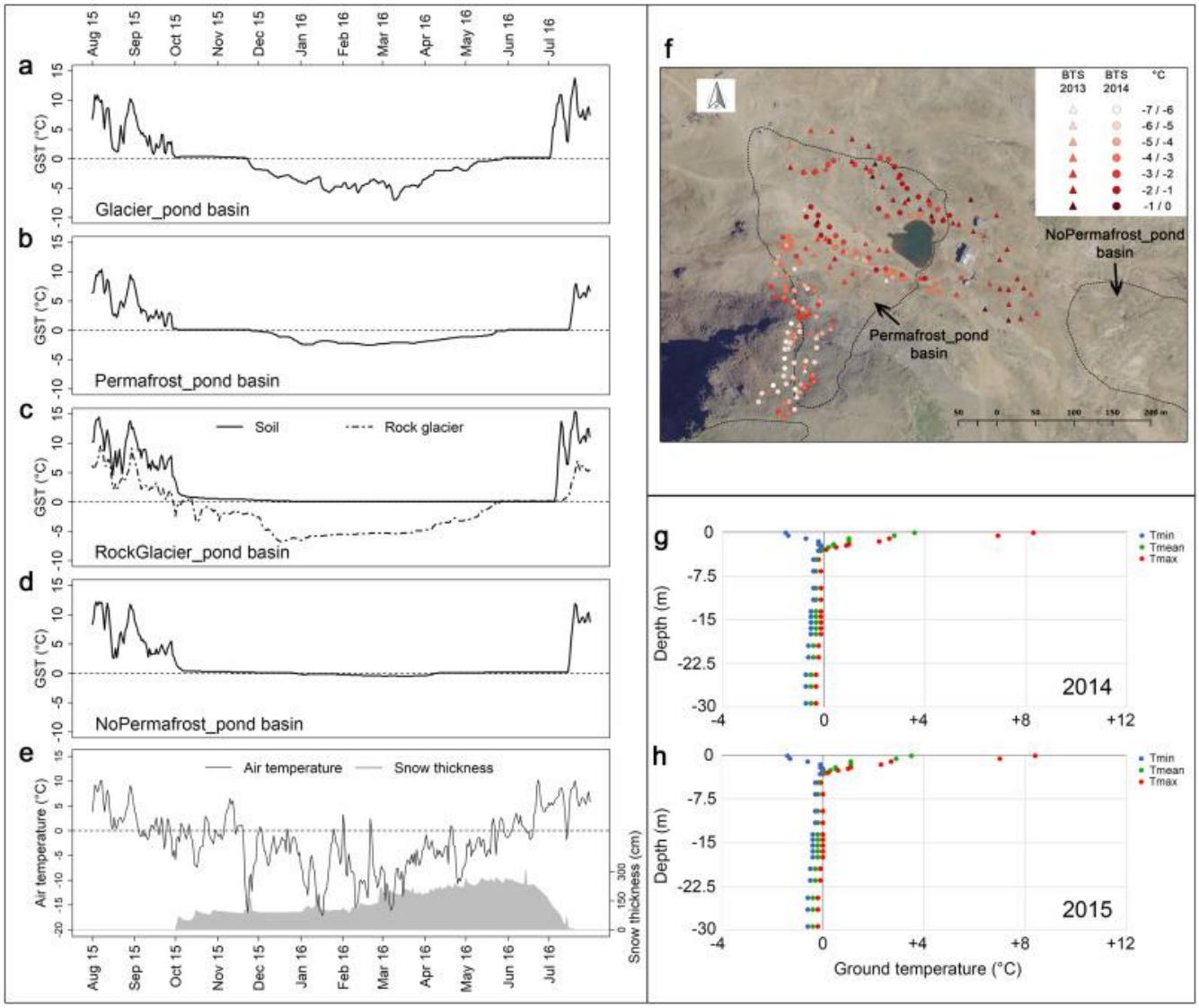

Fig. 4. Thermal regime from the ground surface temperature (GST) measurements in the investigated basins (a–d), compared with (e) air temperature and snow thickness recorded at the Col d'Olen AWS in the time-frame 1 August 2015–31 July 2016; see Fig. 2b1–2b4 for GST sensor locations. (f) Location and temperatures of the bottom temperature of the snow cover (BTS) measurements in 2013 and 2014 in the Permafrost_pond and NoPermafrost_pond basin area. Ground temperature (GT) measured in the 30-m deep borehole of permafrost station managed by Arpa Piemonte in the southern slopes of the Permafrost_pond basin, in 2014 (g) and 2015 (h) (www.alpine-permafrostdata.eu); the location of the borehole is shown in Fig. 2b2.

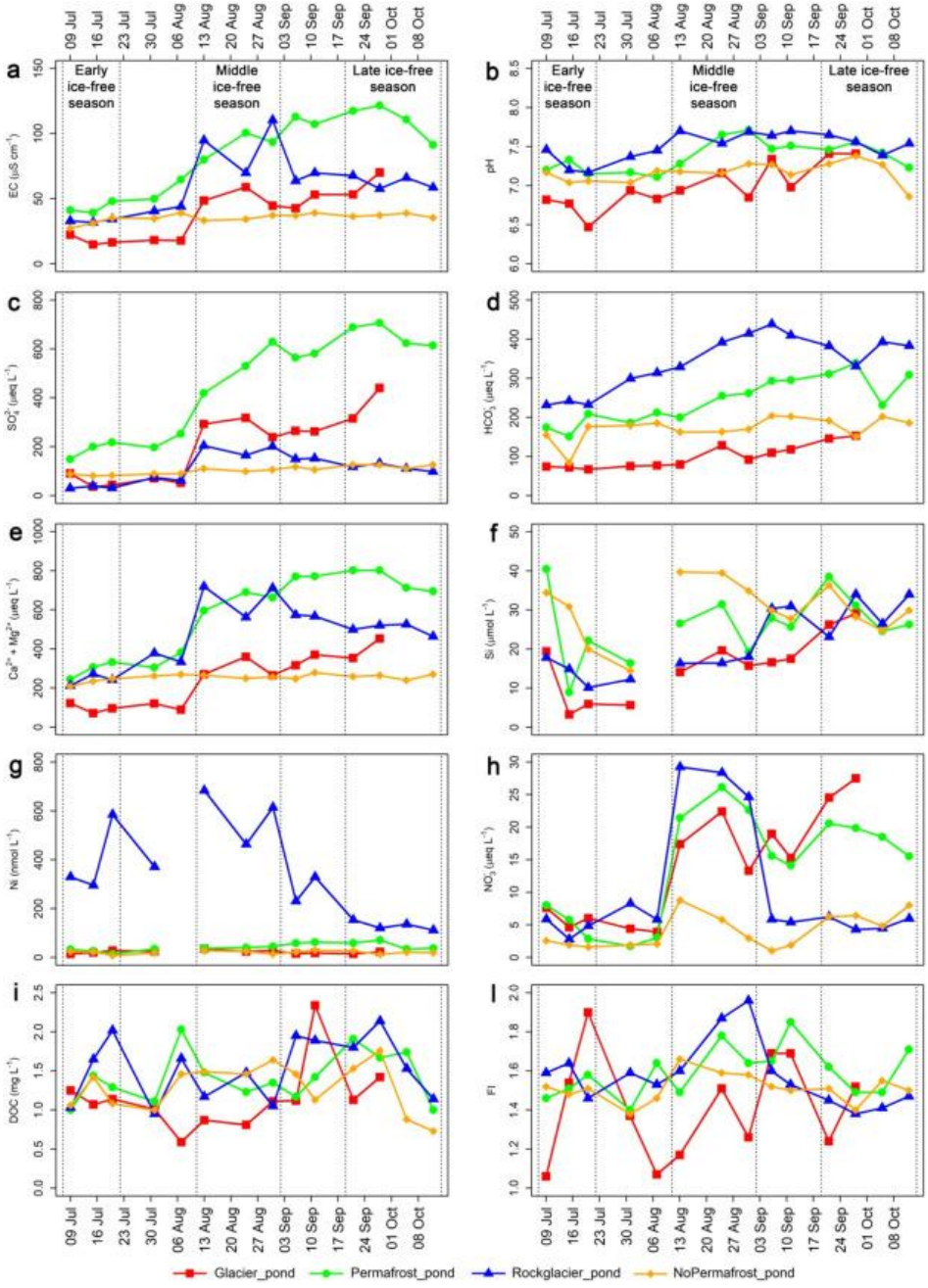

Fig. 5. Seasonal trends of pond water quality and biotic parameters for the 2015 ice-free season. (a) Electrical conductivity (EC), (b) pH, (c) SO42−, (d) HCO3−, (e) Ca2+ + Mg2+, (f) Si, (g) Ni, (h) NO3−, (i) dissolved organic carbon (DOC), and (l) fluorescence index (FI). Early, middle, and late ice-free season periods are also shown.

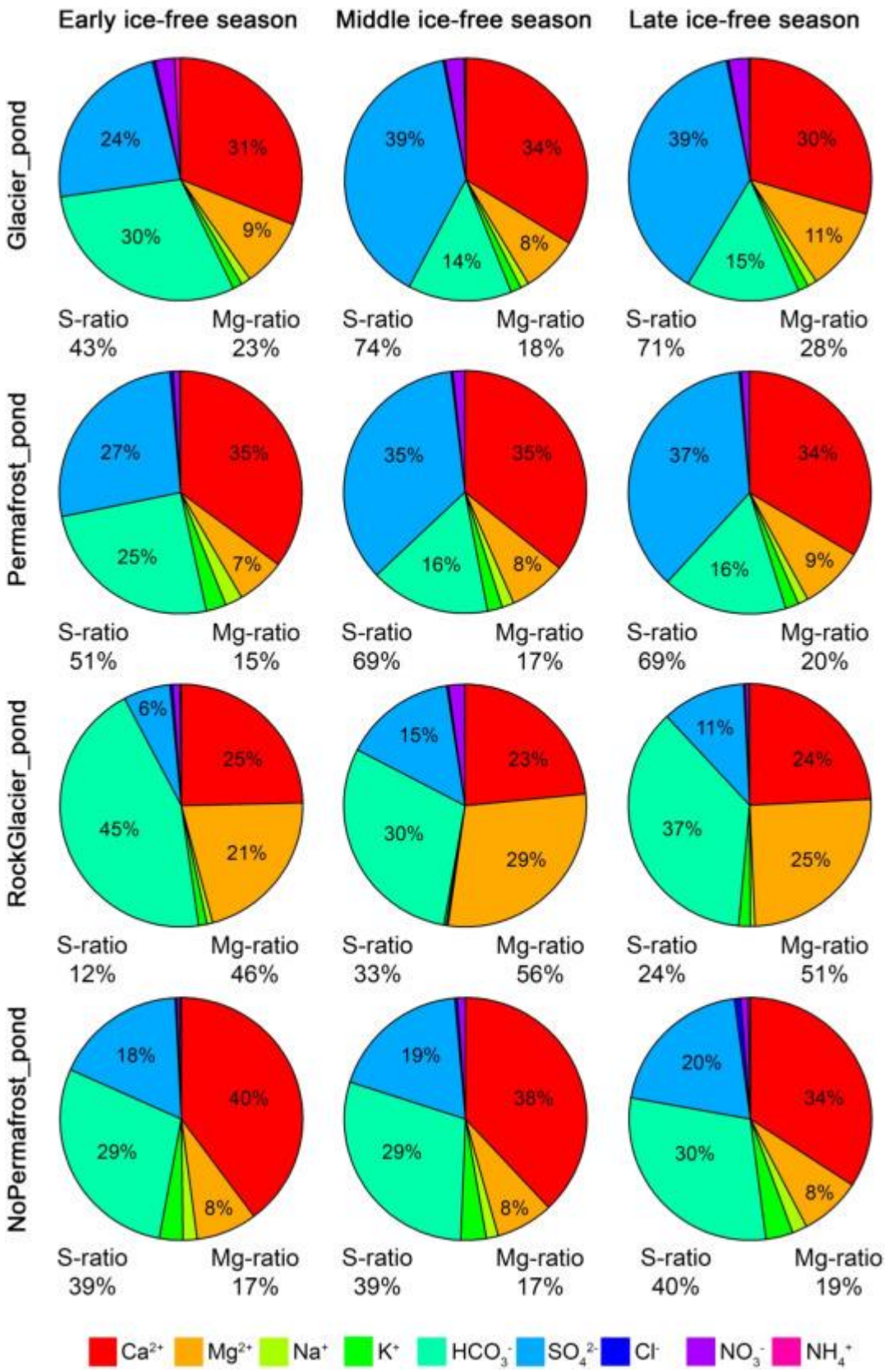

Fig. 6. Relative contribution of the various ions to the total ionic content of the ponds, together with S-ratio and Mg-ratio, during the early, middle and late ice-free season 2015.

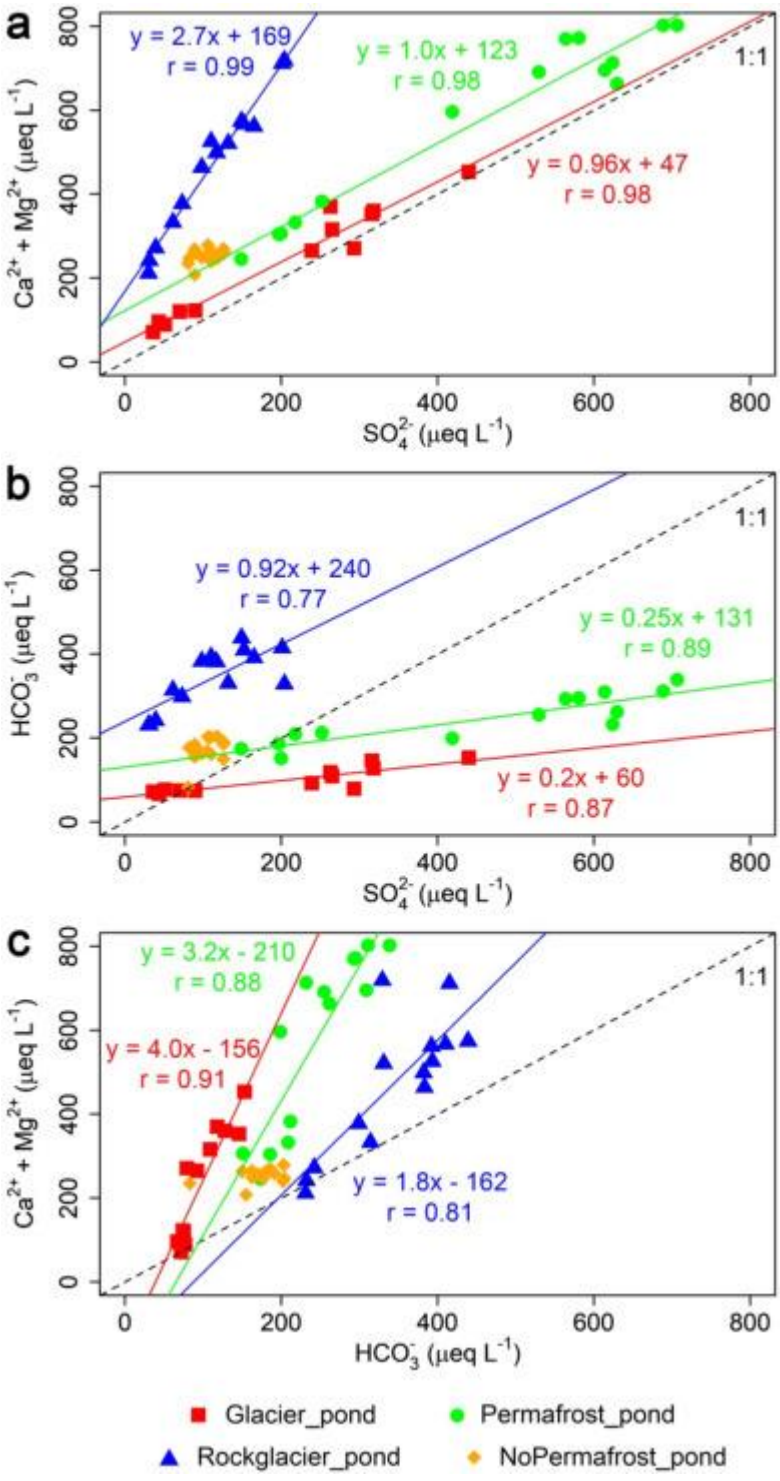

Fig. 7. Ion associations and regression equations for the investigated ponds: (a) (Ca2+ + Mg2+) vs SO42−; (b) HCO3− vs SO42−; (c) (Ca2+ + Mg2+) vs HCO3−. Significant slopes and intercepts between major ions and SO42− are also reported in Table S3.

Supplementary Material for

Influence of permafrost, rock and ice glaciers on chemistry of high-elevation ponds (NW Italian Alps)

N. Colombo[a], F. Salerno[b,*], M. Martin[a], M. Malandrino[c], M. Giardino[d], E. Serra[e], D. Godone[f], D. Said-Pullicino[a], S. Fratianni[d], L. Paro[g], G. Tartari[b], M. Freppaz[a]

[a]University of Turin, Department of Agricultural, Forest and Food Sciences, Grugliasco, Italy.
[b]CNR-IRSA (National Research Council - Water Research Institute), Brugherio, Italy.
[c]University of Turin, Department of Chemistry, Turin, Italy.
[d]University of Turin, Department of Earth Sciences, Turin, Italy.
[e]University of Bern, Institute of Geological Sciences, Bern, Switzerland.
[f]CNR-IRPI (National Research Council - Research Institute for Geo-Hydrological Protection), Turin, Italy.
[g]Arpa Piemonte, Department of "Natural and Environmental Risks", Turin, Italy.

Corresponding author: Franco Salerno (salerno@irsa.cnr.it)

Contents of this file

Region of investigation (S1) and Materials and Methods (S2)
Figures S1 to S2
Tables S1 to S3

S1 Study area

The Glacier_pond basin is dominated by metamorphic rocks with acid composition and schistous texture (paraschists and polimetamorphic schists with minor migmatite bodies). Intrusive and metamorphic rocks, with acid composition, prevalently with massive structure (leucochratic gneiss and metagranites), metamorphic rocks with basic composition and massive texture (metabasites), and minor bodies of metamorphic rocks with a terrigenous-carbonatic composition and schistous texture (calcschists), are also present (Fig. 2a1).

The Permafrost_pond is characterised by outcrops of metamorphic rocks with acid composition and schistous texture (micaschists), intrusive and metamorphic rocks, with acid composition, prevalently with massive structure (gneiss), and metamorphic rocks with basic composition and massive texture (amphibolites, rhodingitic metagabbros) (Fig. 2a2).

The RockGlacier_pond basin is characterised by metamorphic rocks with basic/ultrabasic composition and schistous texture (serpentinites, serpentineschists), metamorphic rocks with basic composition and massive texture (amphibolites), metamorphic rocks with a terrigenous-carbonatic composition and schistous texture (calcschists), and metamorphic rocks with acid composition and schistous texture (paraschists) (Fig. 2a3).

Finally, the lithological setting of the NoPermafrost_pond basin is characterised by metamorphic rocks with acid composition and schistous texture (micaschists), intrusive and metamorphic rocks, with acid composition, prevalently with massive structure (gneiss), metamorphic rocks with basic composition and massive texture (amphibolites), and metamorphic rocks with silica composition and massive structure (Quartzites) (Fig. 2a4).

Geologically, the study area shows a tectonic intersection of major structural/paleogeographic domains of the Alpine orogen, with the presence (from north to south) of the Monte Rosa nappe, the 'Zermatt-Saas' unit, the 'Combin Zone' unit (these two latter being Penninic nappes with distinct metamorphic facies), and the Sesia Lanzo Zone. Especially in the RockGlacier_pond basin, the tectonic contact between the 'Zermatt Sass' unit (eclogite facies) and the overlaying 'Combin Zone' (blueschist facies) unit is characterised by distinctive structural association of brittle faults and fractures (Colombo et al., 2018a and references therein reported). These structural features have been reported to influence mainly the outflowing dynamics of the RockGlacier_pond, through a seepage occurring across a minor fault zone affecting the bedrock at the pond bottom (Colombo et al., 2018a). This distinctive structural association is less evident or absent in the other pond basins, thus the overall geological context is assumed to be similar among the ponds.

S2 Materials and Methods

S2.1 Cryospheric and snow cover features

The Alpine Permafrost Index Map (APIM) shows a qualitative index describing how likely permafrost exists, requiring an interpretation key to further locally refine the estimate shown in the map. For instance, coarse-debris cover is considered among the most important factors indicating cold ground conditions. Conversely, bedrock, soil and vegetation covers are considered as factors indicating warm ground conditions and/or absence of permafrost (Boeckli et al., 2012).

For the ground surface temperature (GST) measurements, miniature sensors Maxim iButton DS1922L (accuracy ±0.5 °C, resolution 0.0625 °C) were used. The sensors were installed at the depth of approximately 5−10 cm below the debris/soil cover (and among the blocks of the rock glacier). Sensors were programmed to record every three hours from 1 August 2015 to 31 July 2016. Three-hourly data were aggregated to daily values. No data gaps were present in the series. The methodology used for waterproofing the sensors is reported in Colombo et al. (2018b). In addition, a thermistor combined with a GEOTEST UTL-1 data logger (accuracy ±0.1 °C, resolution 0.27 °C) measured GST in the

NoPermafrost_pond basin on a hourly basis for the period 2008–2015. Hourly data were aggregated to daily values. No data gaps were present in the series.
To measure the bottom temperature of the snow cover (BTS), a thermometer Delta Ohm RTD HD 2307.0 (accuracy ±0.05 °C, resolution 0.1 °C), equipped with a probe Pt100 TP474C.0, has been installed on a stainless steel probe. The location of each sample point was recorded with a handheld Global Positioning System (GPS) ("Aventura" TwoNav vs. 2.6.2). The measurements were performed during the late winter (March/April), when a sufficient snow cover was established since at least one month, before the onset of snow melt. Since a minimum snow thickness of 80 cm is necessary to provide a sufficient insulation against air temperature variations, measurements were made only where this threshold was found. About 200 measurements were obtained over a range of elevations, aspects, slopes and land covers.
For the snow cover duration analyses, hourly data on snow thickness were obtained from the Col d'Olen station. Data were aggregated to daily values and no data gaps were present in the series. Moreover, Landsat 8 (spatial resolution: 30 m, geolocation uncertainty: 3–6 m, Storey et al., 2014) imagery was analysed. Landsat 8 data were downloaded from https://earthexplorer.usgs.gov by setting the desired time span and by using the basin shapefiles. An R script (R Core Team, 2018) originally developed for analysing MODIS data (Godone et al., 2011; Minora et al., 2015) was used to detect snow cover in each Landsat scene. Every scene was masked with the boundaries of the study area and processed to detect snow covered pixels based on NDSI (Normalized Difference Snow Index, Riggs et al., 1994):

$$NDSI = \frac{band\ 3 - band\ 6}{band\ 3 + band\ 6} \quad (1)$$

where, band 3 has wavelengths of 0.53–0.59 μm (green) and band 6 has wavelengths of 1.57–1.65 μm (short-wavelength infrared). When NDSI was greater than 0.4 the pixel was classified as snow. Concerning the Glacier_pond basin, an additional processing was carried out in order to remove, from the basin surface, the Indren Glacier area. The aim of the editing was to remove ice covered surface which may distort the quantification of snow covered surface. Glacier outline was plotted by the employment of the orthoimage of the year 2012 as base layer. Its surface was then subtracted, in GIS environment, from the basin shapefile. The corrected shapefile was then used in the computation. The classified raster was then converted into tabular form for counting and quantification of snow cover duration in the catchment.

S2.2 Pond water and precipotation sampling, and chemical analyses

High-mountain lacustrine waters contain very low solute concentrations, it is therefore imperative that sampling, storage and analysis are done with extreme care to avoid false positive results or high blanks. Measurements were performed in triplicates. For every sampling date and at each sampling point, samples were collected in new polyethylene tubes that had been rinsed several times with high-purity Milli-Q water. To properly choose the tubes used for the sampling, they were preliminarily tested, storing Milli-Q water as well as acidified water in conditions similar to those of the samples. No release of the analysed solutes was detected. For chromatographic analysis of major anions, the content of the tubes was immediately filtered through a 0.2 μm membrane filter. Another aliquot of the filtered samples was acidified to pH<2 with hydrochloric acid, purified by sub-boiling distillation, and used for analysis of major cations and trace elements. The first 15-20 ml of the filtrate in the tubes was discarded to condition the filter and then the tubes were pre-rinsed three times with filtered sample water. Samples for major and trace elements were processed in a clean environment under a Class-100 laminar-flow bench-hood. The sample blanks were prepared similarly to samples in the laboratory,

without the field sampling step. Since the difference between the sample blanks and the calibration blanks was always lower than the detection limit of the used instrument, the calibration blank, made in connection with instrumental calibration and daily prepared, was subtracted from the sample concentration. Also, the standard solutions for the instrumental calibration were prepared in aliquots of calibration blank. The tubes used for measurements of electrical conductivity (EC), pH, dissolved organic carbon (DOC), dissolved inorganic carbon (DIC), and fluorescence index (FI), remained unfiltered and were pre-rinsed three times with sample water. An aliquot of the unfiltered samples was filtered in the laboratory through a 0.45 µm filter, the filtered aliquot was then transferred and stored in acid-washed and combusted glass vials at +4 °C in the dark, and subsequently analysed for DOC, DIC, and FI. Samples were stored in an ice-packed cooler (KERN FRIO Diagnosach) during transport and immediately transferred to the laboratory where they were refrigerated (at +4 °C). Snow samples were stored frozen (at -20 °C) until analysis, then placed in covered polyethylene buckets and melted at room temperature. DOC was determined on acidified sample aliquots using Pt-catalysed, high temperature combustion followed by infrared detection of CO_2, after removing inorganic C by purging. FI samples were scanned in an optically clear quartz cuvette. Scans were performed at an excitation wavelength of 370 nm, for emissions wavelengths between 370 and 700 nm at 1-nm increments. Scans of sample blanks of deionised water were performed, and the blank fluorescence values were subtracted from the raw scans of the samples in order to remove the effects of Raman scattering (Lafrenière and Sharp, 2004). After subtracting the blank, the fluorescence index (FI-the ratio of emission intensity at 450 nm to 500 nm for an excitation of 370 nm) was determined (McKnight et al., 2001). Limit of detection (LOD) and limit of quantification (LOQ) of the analytes were as follows: Cl^-, LOD > 0.5 µeq L^{-1} / LOQ > 1.7 µeq L^{-1}; SO_4^{2-}, LOD > 4 µeq L^{-1} / LOQ > 13.3 µeq L^{-1}; NO_3^-, LOD > 1 µeq L^{-1} / LOQ > 3.3 µeq L^{-1}; NO_2^-, LOD > 0.5 µeq L^{-1} / LOQ > 1.7 µeq L^{-1}; PO_4^{3-}, LOD > 4 µeq L^{-1} / LOQ > 13.3 µeq L^{-1}; DIC (as HCO_3^-), LOD > 4.2 µeq L^{-1} / LOQ > 14 µeq L^{-1}; Ca^{2+}, LOD > 2.5 µeq L^{-1} / LOQ > 8.3 µeq L^{-1}; Mg^{2+}, LOD > 0.8 µeq L^{-1} / LOQ > 2.7 µeq L^{-1}; Na^{2+}, LOD > 1.5 µeq L^{-1} / LOQ > 5 µeq L^{-1}; K^{2+}, LOD > 1.3 µeq L^{-1} / LOQ > 4.3 µeq L^{-1}; Si, LOD > 0.5 µmol L^{-1} / LOQ > 1.7 µmol L^{-1}; Ni, LOD > 0.62 nmol L^{-1} / LOQ > 2.1 nmol L^{-1}; Mn, LOD > 1.3 nmol L^{-1} / LOQ > 4.3 nmol L^{-1}; Co, LOD > 0.17 nmol L^{-1} / LOQ > 0.57 nmol L^{-1}; DOC, LOD > 0.05 mg L^{-1} / LOQ > 0.17 mg L^{-1}. NH_4^+ was calibrated between 0.025 and 0.5 mg L^{-1}.

Figures and tables

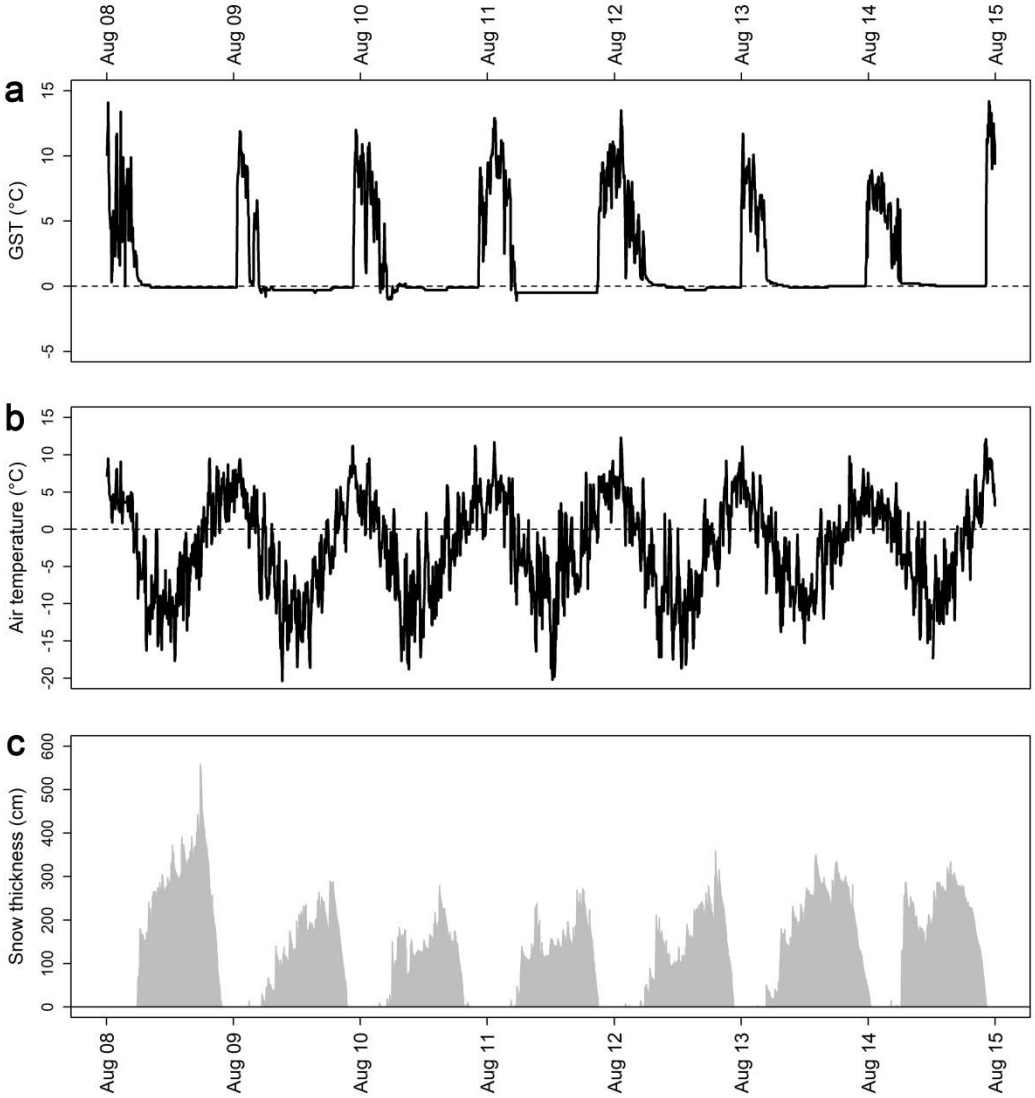

Fig. S1 – (a) Ground surface temperature (GST) regime at the NoPermafrost_pond basin (period 2008–2015), compared with (b) air temperature and (c) snow thickness recorded at the Col d'Olen AWS (2900 m a.s.l.).

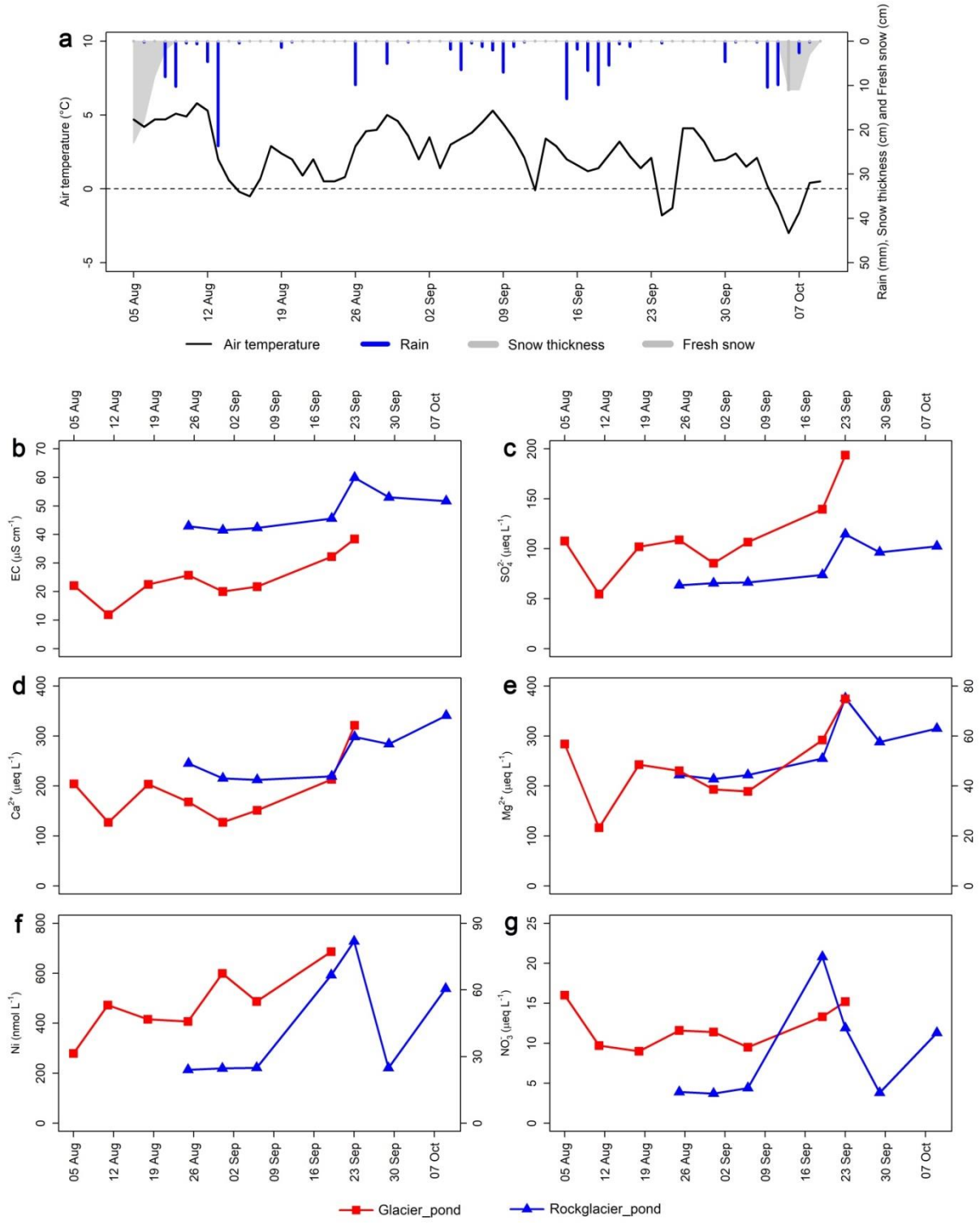

Fig. S2 – Ice-free season 2014. (a) Air temperature (°C), mean daily rain (mm), fresh snow (cm) and snow thickness (cm). (b) Electrical conductivity (EC) at Glacier_pond and RockGlacier_pond, (c) SO_4^{2-}, (d) Ca^{2+}, (e) Mg^{2+}, (f) Ni, (g) NO_3^-. In e and f the Glacier_pond is represented on the secondary y axis. The Permafrost_pond and NoPermafrost_pond were not sampled in the ice-free season 2014.

Parameter	Sampling site	Early ice-free season (E)	Middle ice-free season (M)	Late ice-free season (L)	Difference (%) (M-E)/E	Difference (%) (L-E)/E
EC (µS cm^{-1}, 20 °C)	Glacier_pond	18 (4)	51 (7)	62 (12)	**+184**	**+246**
	Permafrost_pond	43 (5)	91 (11)	110 (13)	**+113**	**+157**
	RockGlacier_pond	33 (1)	92 (21)	63 (5)	**+178**	**+89**
	NoPermafrost_pond	31 (4)	35 (2)	37 (2)	+12	**+18**
H_3O^+ (nmol L^{-1})	Glacier_pond	220 (103)	108 (36)	39 (0)	-51	-82
	Permafrost_pond	60 (12)	31 (18)	40 (13)	**-48**	**-34**
	RockGlacier_pond	55 (18)	23 (5)	30 (8)	**-58**	**-46**
	NoPermafrost_pond	82 (13)	63 (9)	71 (45)	**-24**	-13
SO_4^{2-} (µeq L^{-1})	Glacier_pond	56 (29)	283 (41)	378 (88)	**+402**	**+569**
	Permafrost_pond	189 (36)	526 (105)	658 (46)	**+179**	**+249**
	RockGlacier_pond	33 (5)	190 (22)	114 (14)	**+476**	**+247**
	NoPermafrost_pond	84 (4)	105 (6)	122 (8)	**+25**	**+45**
HCO_3^- (µeq L^{-1})	Glacier_pond	71 (4)	100 (25)	149 (5)	+41	**+111**
	Permafrost_pond	178 (29)	239 (34)	298 (46)	+34	**+67**
	RockGlacier_pond	235 (6)	379 (44)	373 (28)	**+61**	**+58**
	NoPermafrost_pond	138 (49)	165 (4)	183 (22)	+20	+32
Ca^{2+} (µeq L^{-1})	Glacier_pond	74 (18)	244 (43)	292 (51)	**+215**	**+277**
	Permafrost_pond	248 (27)	536 (26)	600 (57)	**+116**	**+142**
	RockGlacier_pond	130 (8)	298 (69)	245 (17)	**+129**	**+90**
	NoPermafrost_pond	191 (22)	214 (4)	208 (13)	+12	+9
Mg^{2+} (µeq L^{-1})	Glacier_pond	22 (8)	55 (11)	111 (20)	**+149**	**+404**
	Permafrost_pond	46 (19)	114 (28)	153 (11)	**+146**	**+231**
	RockGlacier_pond	112 (25)	366 (22)	256 (22)	**+227**	**+129**
	NoPermafrost_pond	39 (2)	43 (5)	50 (6)	+11	**+28**
Ca^{2+} + Mg^{2+} (µeq L^{-1})	Glacier_pond	83 (25)	312 (53)	403 (71)	**+275**	**+383**
	Permafrost_pond	294 (45)	650 (48)	753 (57)	**+121**	**+156**
	RockGlacier_pond	242 (30)	664 (89)	503 (28)	**+175**	**+108**
	NoPermafrost_pond	230 (20)	257 (8)	258 (13)	+12	+12
Si (µmol L^{-1})	Glacier_pond	10 (9)	16 (3)	28 (2)	+73	+190
	Permafrost_pond	24 (16)	26 (6)	30 (6)	+8	+26
	RockGlacier_pond	14 (4)	17 (1)	29 (6)	+18	**+106**
	NoPermafrost_pond	28 (8)	38 (3)	30 (5)	+34	+5
Ni (nmol L^{-1})	Glacier_pond	21 (7)	29 (6)	19 (5)	+42	−10
	Permafrost_pond	24 (9)	41 (4)	50 (17)	+69	+106
	RockGlacier_pond	403 (158)	587 (113)	131 (19)	+46	**−68**
	NoPermafrost_pond	18 (9)	22 (7)	18 (6)	+21	−3
NO_3^- (µeq L^{-1})	Glacier_pond	6 (2)	18 (5)	26 (2)	**+191**	**+327**
	Permafrost_pond	6 (3)	23 (3)	19 (2)	**+321**	**+235**

	RockGlacier_pond	5 (2)	27 (3)	5 (1)	**+508**	+16
	NoPermafrost_pond	2 (1)	6 (3)	6 (1)	**+191**	**+217**
DOC (mg L^{-1})	Glacier_pond	1.2 (0.1)	0.9 (0.2)	1.3 (02)	−19	+11
	Permafrost_pond	1.2 (0.2)	1.4 (0.1)	1.6 (0.4)	+9	+27
	RockGlacier_pond	1.6 (0.5)	1.2 (0.2)	1.7 (0.4)	−21	+6
	NoPermafrost_pond	1.2 (0.2)	1.5 (0.1)	1.2 (0.5)	**+29**	+3
FI	Glacier_pond	1.5 (0.4)	1.3 (0.2)	1.4 (0.2)	−13	−8
	Permafrost_pond	1.5 (0.1)	1.6 (0.1)	1.6 (0.1)	+8	+4
	RockGlacier_pond	1.6 (0.1)	1.8 (0.2)	1.4 (0.1)	+16	**−9**
	NoPermafrost_pond	1.5 (0.1)	1.6 (0.1)	1.5 (0.1)	+7	−1

Table S1 – Mean values of electrical conductivity (EC), pH (here expressed as H_3O^+), selected solute and dissolved organic carbon (DOC) concentrations, and fluorescence index (FI) at the survey ponds sampled during the early, middle and late ice-free season. The standard deviation is in brackets.

Parameter	Glacier_pond (Coarse sediment) 2015–2016	Permafrost_pond (Coarse sediment) 2015–2016	RockGlacier_pond (Rock glacier) 2015–2016	RockGlacier_pond (Soil) 2015–2016	NoPermafrost_pond (Soil) 2015–2016	NoPermafrost_pond (Soil) 2008–2015
MAGST (°C)	–0.1	+0.3	–1.6	+2.4	+1.6	+1.7
GFI (°C·day)	–593	–294	–912	0	−27	−42
WEqT (°C)	/	–2.2	–5.5	+0.1	−0.2	−0.5 ÷ 0

Table S2 – Relevant parameters extracted from the ground surface temperature (GST) data. MAGST: mean annual ground surface temperature; GFI: ground freezing index; WEqT: winter equilibrium temperature. The WEqT was not reached at the monitoring site of the Glacier_pond due to the scarce and discontinuous snow cover because of snow depletion by wind.

Pond	Ion association		
	$(Ca^{2+} + Mg^{2+})$ *vs* SO_4^{2-}	HCO_3^- *vs* SO_4^{2-}	$(Ca^{2+} + Mg^{2+})$ *vs* HCO_3^-
Glacier_pond	0.96 (47)	0.20 (60)	4 (-156)
Permafrost_pond	1.00 (122)	0.25 (131)	3.2 (-210)
RockGlacier_pond	2.70 (170)	0.92 (240)	1.8 (-162)

Table S3 – Simple linear regression equations between major ions. Slopes and intercepts (in brackets) are reported only for significant ($p < 0.05$) regression equations. Regressions are shown in Fig. 7.

Supplementary references

Boeckli, L., Brenning, A., Gruber, S., Noetzli, J., 2012. Permafrost distribution in the European Alps: calculation and evaluation of an index map and summary statistics. Cryosphere 6, 807–820.

Colombo, N., Sambuelli, L., Comina, C., Colombero, C., Giardino, M., Gruber, S., Viviano, G., Vittori Antisari, L., Salerno, F., 2018a. Mechanisms linking active rock glaciers and impounded surface water formation in high-mountain areas. Earth. Surf. Process. Landf. 43(2), 417–431.

Colombo, N., Gruber, S., Martin, M., Malandrino, M., Magnani, A., Godone, D., Freppaz, M., Fratianni, S., Salerno, F., 2018b. Rainfall as primary driver of discharge and solute export from rock glaciers: The Col d'Olen Rock Glacier in the NW Italian Alps. Sci. Total Environ. 639, 316–330.

Godone, D., Garnero, G., Filippa, G., Freppaz, M., Terzago, S., Rivella, E., Salandin, A., Barbero, S, 2011. Snow cover extent and duration in MODIS time series: A comparison with in-situ measurements (Provincia Verbano Cusio Ossola, NW Italy). International Conference on Multimedia Technology, IEEE. doi:10.1109/ICMT.2011.6002893.

Lafrenière, M.J., Sharp, M.J., 2004. The concentration and fluorescence of dissolved organic carbon (DOC) in glacial and nonglacial catchments: Interpreting hydrological flow routing and DOC sources. Arct. Antarct. Alp. Res. 36, 156–165.

McKnight, D.M., Boyer, E.W., Westerhoff, P.K., Doran, P.T., Kulbe, T., Andersen, D.T., 2001. Spectrofluorometric characterization of dissolved organic matter for indication of precursor organic material and aromaticity. Limnol. Oceanogr. 46, 38–48.

Minora, U., Godone, D., Lorenzini, S., D'agata, C., Bocchiola, D., Sepulveda Barcaza, G., Smiraglia, C., Diolaiuti, G., 2015. 2008-2011 Snow Covered Area (SCA) variability over 18 watersheds of the central Chile through MODIS data. Geogr. Fis. Din. Quat. 38(2), 169–174.

R Core Team, 2019. R: A language and environment for statistical computing. R Foundation for Statistical Computing, Vienna, Austria. URL https://www.R-project.org/ (date of access 24th April 2019)

Riggs, G.A., Hall, D.K., Salomonson, V.V., 1994. A snow index for the Landsat Thematic Mapper and Moderate Resolution Imaging Spectroradiometer. Proceedings of IGARSS '94 - 1994 IEEE International Geoscience and Remote Sensing Symposium 4, 1942–1944.

Storey, J., Choate, M., Lee, K., 2014. Landsat 8 operational land imager on-orbit geometric calibration and performance. Remote Sens. 6(11), 11127–11152.